Context-dependent representations of objects and space in the primate hippocampus during virtual navigation

Roberto A. Gulli [1,2,3,4]*, Lyndon R. Duong [2,10], Benjamin W. Corrigan [1,2], Guillaume Doucet [2,5,11], Sylvain Williams[6], Stefano Fusi [3,4,7] and Julio C. Martinez-Trujillo [2,8,9]*

The hippocampus is implicated in associative memory and spatial navigation. To investigate how these functions are mixed in the hippocampus, we recorded from single hippocampal neurons in macaque monkeys navigating a virtual maze during a foraging task and a context–object associative memory task. During both tasks, single neurons encoded information about spatial position; a linear classifier also decoded position. However, the population code for space did not generalize across tasks, particularly where stimuli relevant to the associative memory task appeared. Single-neuron and population-level analyses revealed that cross-task changes were due to selectivity for nonspatial features of the associative memory task when they were visually available (perceptual coding) and following their disappearance (mnemonic coding). Our results show that neurons in the primate hippocampus nonlinearly mix information about space and nonspatial elements of the environment in a task-dependent manner; this efficient code flexibly represents unique perceptual experiences and correspondent memories.

The hippocampus is a phylogenetically ancient structure of the mammalian cortex that has been shown to play an important role in memory and spatial navigation. Theoretical attempts to reconcile these functions have led some groups to suggest a primacy for spatial coding in the hippocampus[1–3]; others have suggested that the fundamental role of the hippocampus is memory, with physical space as just one variable that must be conjunctively encoded in episodic memory[4,5]. Direct comparisons of spatial and nonspatial representations in hippocampal neurons are challenging because of methodological gaps between model species[1,5–7]. Furthermore, extrapolating hippocampal coding schemes across species is complicated by the diverse organizations of sensory systems and resultant reorganization of sensory inputs to the hippocampus[8,9].

A wealth of experimental and incidental lesion literature has implicated the hippocampus in associative memory across species[10]. In humans and nonhuman primates some hippocampal neurons have been shown to differentially respond to unfamiliar and familiar objects at certain locations[11–13]; responses during initial presentation are predictive of subsequent recognition[14]. Furthermore, changes in the selectivity of hippocampal neurons correlate with performance changes[15] and trial outcome during associative memory tasks[16,17].

In rodents, the discovery of place cells that fire action potentials when animals occupy a specific location in an environment[18] implicated the hippocampus in spatial navigation[19]. In primates, analogous neurons have been reported, although these may be modulated in ways that are species-specific. Several studies that account for gaze position suggest that spatially specific firing in hippocampal neurons is dependent on spatial view in monkeys[20] and

humans[21,22]. Hippocampal place fields are sensitive to the configuration of extramaze cues in monkeys[23], while the activity of some neurons is invariant to changes in the identity of distal environmental cues and seems to encode their position relative to goal locations[24]. Primate hippocampal activity may also be dependent on the previous sequence of events before entering the place field[25]. Individual neurons in the primate hippocampus may fire in a spatially specific manner but their activity is qualitatively distinct from place cells observed in rodents; primate hippocampal neurons with spatial firing seem to be modulated by view, environmental, cognitive and behavioral factors[9].

An emergent view from this body of research is that some individual neurons in the primate hippocampus exhibit selectivity for elements of associative memory and some neurons fire in a spatially specific manner. These activity patterns could be carried out by separable populations of neurons, or a single population of neurons may carry spatial and nonspatial information. The extent to which this information may mix, and how sensory and mnemonic components of cognitive tasks can drive spatial specificity, have not been extensively investigated in primates. To examine these issues, one would need to first examine the activity of single neurons across different behavioral tasks in a common space. Second, spatial and nonspatial features of the environment must be parameterized and regressed against neural activity. Third, one must analyze not only the information encoded by single neurons[26] but apply multivariate analysis techniques that consider the multidimensional nature of the information encoded by populations of neurons[27,28].

[1]Integrated Program in Neuroscience, McGill University, Montréal, Quebec, Canada. [2]Robarts Research Institute, Western University, London, Ontario, Canada. [3]Mortimer B. Zuckerman Mind Brain Behavior Institute, Columbia University, New York, NY, USA. [4]Center for Theoretical Neuroscience, Columbia University, New York, NY, USA. [5]Department of Physiology, McGill University, Montréal, Quebec, Canada. [6]Department of Psychiatry, Douglas Research Center, McGill University, Montréal, Quebec, Canada. [7]Kavli Institute for Brain Sciences, Columbia University, New York, NY, USA. [8]Brain & Mind Institute, Western University, London, Ontario, Canada. [9]Schulich School of Medicine & Dentistry, Western University, London, Ontario, Canada. [10]Present address: Center for Neural Science, New York University, New York, NY, USA. [11]Present address: Ottawa Hospital Research Institute, Ottawa, Ontario, Canada. *e-mail: roberto.gulli@mail.mcgill.ca; julio.martinez@robarts.ca

To this end, we recorded the activity of single neurons from the right posterior hippocampi of rhesus macaques (*Macaca mulatta*) while they completed two navigation tasks in a single virtual environment: first, an associative memory task; second, a cue-guided foraging task. In both tasks, neurons showed spatial response fields; a linear classifier reliably decoded the animal's position in the maze from the population activity. However, the population code for space did not generalize across tasks in the same environment, indicating that the spatial codes for the environment were task-specific. To explain this lack of generalization, task-specific activity was examined in the portion of the maze where the population code for space was most divergent across tasks. We found that hippocampal neurons encoded nonspatial features of the associative memory task (that is, contexts and objects) when they were visible in the environment and encoded these features mnemonically after they were removed from the environment. Finally, using the population activity, we decoded unique combinations of nonspatial features in single trials.

Results

Single-neuron spatial information content (SIC) during each task in the X-Maze. In these experiments, monkeys were seated in a custom-built chair in front of a computer monitor and used a two-axis joystick to complete tasks that required navigation through a virtual reality environment called the X-Maze[29] (Fig. 1a). While monkeys completed these tasks, we recorded the activity from 183 individual neurons from the superior aspect of the right mid-posterior hippocampus (predominantly CA3; see Fig. 1b, Extended Data Fig. 1, Extended Data Fig. 2 and Methods). Trajectories were planned and verified during electrode insertion using magnetic resonance imaging (MRI)-guided neuronavigation (Fig. 1b and Extended Data Fig. 1).

The first task monkeys completed was an associative memory task. Animals had to navigate to objects in the virtual environment in a context-dependent manner (Fig. 1c, Extended Data Fig. 3 and Supplementary Video 1). The objects were colored disks that appeared at the ends of the X-Maze on each trial. The context was defined by a texture applied to the maze walls. Each trial of the associative memory task started in one end of the maze and included five distinct trial epochs that occurred as animals navigated toward the objects at the other end of the maze (in order: postreward, precontext, context appearance, object appearance, object approach; see Fig. 1c, Extended Data Fig. 3 and Methods). For analytical purposes, we defined the trial end to be triggered when the subject reached the goal object. The trial start was triggered after the reward was delivered. However, from the monkey's perspective, navigation through the maze was continuous. There was no break or intertrial interval. During the postreward and precontext epochs, all maze walls were gray and no rewarded goals were visible. When the animal entered the central corridor, the 'context appearance' epoch began; the trial context was cued by applying a wood or steel texture to the walls of the corridor and arms of the maze (Extended Data Fig. 3b,c, position a). When animals reached the branched point on the opposite side of the maze (Extended Data Fig. 3b,c, position b), one of the three potentially rewarded colored disks appeared in each arm of the maze. This initiated the 'object appearance' epoch. The animal could examine the objects in either arm of the maze freely and made a choice to navigate toward one of the objects. The first turn toward

the chosen object triggered the start of the 'object approach' epoch, which ended when the monkey reached the goal.

The context and the two objects were selected randomly on every trial. In every session, a new set of three colored disks was used with the same two contexts. Thus, a new conditional association between context and objects was learned daily. Using a Bayesian state–space analysis to estimate the learning state based on the binary trial outcomes (see Methods), we estimated that the context-dependent association between the highest and lowest object was learned after an average of 59 trials across sessions (Extended Data Fig. 3d).

The second task monkeys performed each session was a foraging task. In the foraging task, animals navigated through the X-Maze toward a red volume to receive a juice reward (Fig. 1c and Supplementary Video 2). The red volume was randomly assigned to one of 84 locations in the maze and randomly repositioned at a different location every time the animal reached it. Importantly, the virtual environment was unchanged across tasks.

A variety of spatial firing distributions could be seen across recorded neurons and across tasks (see Fig. 1d and Extended Data Fig. 4 for examples). Such changes were not due to changes in neuronal isolation across tasks (Extended Data Fig. 2). To characterize whether individual neurons fired preferentially in certain parts of the virtual environment, the X-Maze was spatially binned into an isometric, two-dimensional pixel grid covering the entire maze. This pixel grid was used to compute the SIC of each neuron, which quantifies how many bits of information about the location of the animal are transmitted per action potential[30–32]. Shuffled control SIC values were computed by circularly shifting the spike times relative to the spatial positions for each trial; shuffled SIC was subtracted from empirical SIC to yield a normalized SIC value (see Methods).

The distributions of normalized SIC values were not the same across tasks (Fig. 1e; two-sample Kolmogorov–Smirnov test, $P = 2.4 \times 10^{-8}$). In the associative memory task, 76.0% of neurons (139 out of 183) showed significant SIC. In the foraging task, 27.3% of neurons (50 out of 183) had significant SIC. Even among neurons with significant spatial information, the distribution of SIC values was not the same across tasks (two-sample Kolmogorov–Smirnov test, $P = 0.013$). This suggests that neurons contained more spatial information during the associative memory task than during the foraging task in the X-Maze.

In addition, we examined whether individual neurons had spatial response fields in the X-Maze by determining whether firing rates were elevated in any of the maze pixels using a permutation test (see Methods). The number of neurons with firing rates that were statistically elevated for each pixel in each task can be seen in Fig. 2. The X-Maze was then divided into nine similarly sized areas for further analyses (four maze arm areas, two branch areas, three corridor areas). Spatial response fields for each neuron were defined as any of the nine maze areas with statistically elevated firing in one or more pixels. In the associative memory task, 70.0% of neurons had spatial response fields. In contrast with the foraging task, spatial response fields were not uniformly distributed throughout the X-Maze ($P < 1 \times 10^{-7}$, $\chi^2(8) = 52.3$; Fig. 2a, left). In the foraging task, 55.7% of neurons had spatial response fields in at least one maze area (102 out of 183 neurons) with a uniform distribution throughout the maze ($P = 0.91$, $\chi^2(8) = 3.29$; Fig. 2a, right). The distribution of pixels with significantly elevated firing rates in each task, as well as comparisons of individual neuron place field

Fig. 1 | Behavioral tasks and individual neuron SIC. a, Monkeys were seated in front of a computer monitor and used a two-axis joystick to navigate through the virtual reality X-Maze and complete two different tasks. **b**, Recording locations from the right hippocampi (green reconstruction) of two monkeys. Scale bars, 5 mm. **c**, Overhead view of the X-Maze and the animal's trajectory through the maze on two consecutive trials in the associative memory and foraging tasks. **d**, Trajectory (transparent gray) and spike locations (transparent red dots) for six example neurons in both tasks in the X-Maze. **e**, Cumulative distribution of SIC values for all neurons (*n* = 183 per task) showed a statistical difference across tasks (two-sample Kolmogorov–Smirnov test; two-sided $P < 10^{-7}$).

locations within and across tasks with pixel sizes four times larger, were qualitatively unchanged (Extended Data Fig. 5). From these two complementary analyses, it is clear that some neurons encode information about the position of the animal in the maze, and there may be differences in the information content of the population of neurons across tasks.
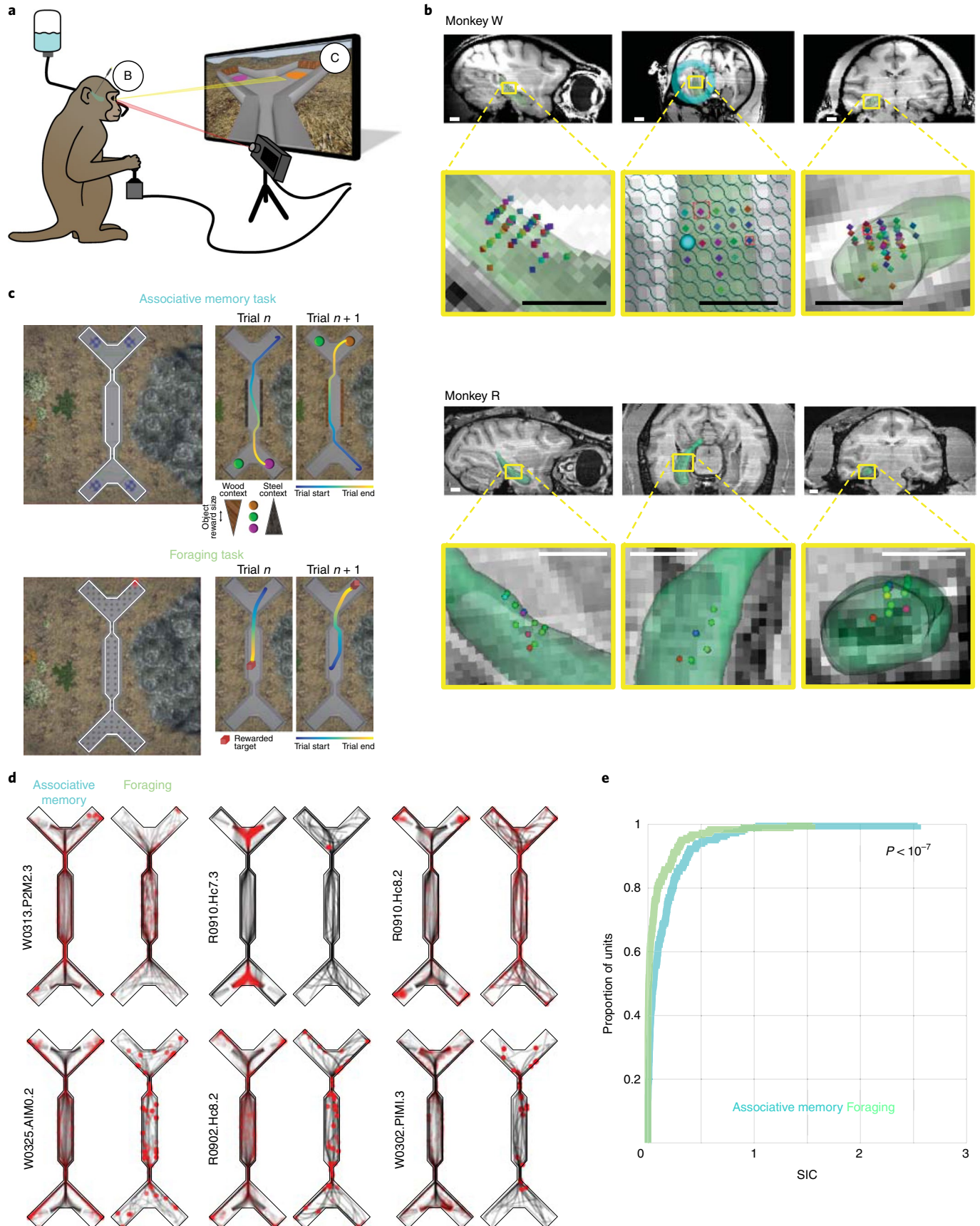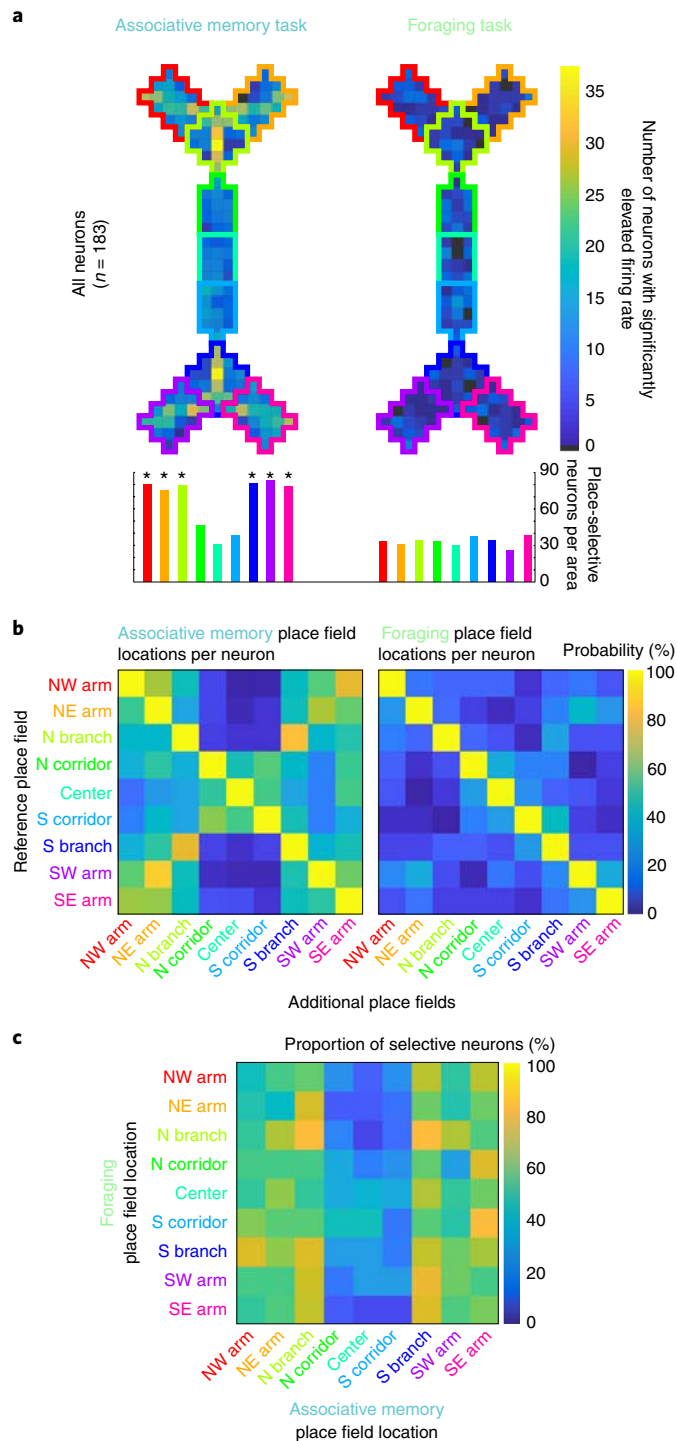
Fig. 2 | Single-neuron spatial response fields in each task. a, Spatial histogram showing the number of neurons with a statistically elevated firing rate in each pixel in both tasks (top). The summarized histogram (bottom) shows the number of neurons with at least one significant pixel in each maze area. The asterisks indicates significantly different proportions across tasks. McNemar's test of equal proportions; Bonferroni-corrected $P < 0.05$. **b,** Locations of coincident place fields for all neurons with more than one place field in each task. **c,** Location of coincident place fields for all neurons with at least one place field in each task. N, north; S, south; W, west; E, east.

Population-level decoding of space within versus across tasks in the X-Maze. The previous results show that individual neurons encode information about space in each task. However, statistical

descriptions of selectivity in single neurons cannot capture the wealth of information encoded by neural populations with mixed selectivity[26–28]. Furthermore, the stability of a population code for space and the optimal spatial reference frame cannot be assessed in single neurons. To better address these questions, we used the firing rates from the entire population of recorded neurons to decode animal position in the X-Maze.

We used a multiclass support vector machine classifier with a linear kernel to decode the animal's position in space using neuronal firing rates (see Methods). This was done using allocentric and egocentric (direction-dependent) spatial reference frames (Fig. 3a) to yield empirical (Fig. 3b, colored distributions) and shuffled control (Fig. 3b, gray distributions) decoding accuracies. Statistical differences between accuracy distributions were assessed via a Wilcoxon rank-sum test (see Methods).

The classifier predicted position in the maze above chance levels in the associative memory task using an allocentric spatial reference frame (Fig. 3b; $24.0 \pm 5.8\%$ accuracy versus $10.8 \pm 4.1\%$ shuffled control accuracy; $P < 10^{-31}$). However, accuracy was poor (Cohen's $\kappa = 0.15$; Methods). The classifier systematically confounded structurally similar areas of the maze, as evidenced by the X-shaped distribution of predictions in the allocentric decoder confusion matrix (Fig. 3c, left). When classification was done using the egocentric reference frame, decoding accuracy improved ($P < 10^{-10}$ compared to allocentric; $58.4 \pm 9.3\%$ versus $19.4 \pm 7.2\%$ shuffled control accuracy; Fig. 3b, second column). The improved accuracy of a population of hippocampal neurons with a direction-dependent reference frame is consistent with previous findings across species[33].

In the foraging task, decoding accuracy was above chance using both reference frames. Decoding accuracy was poor using an allocentric reference frame (Fig. 3b, third column: $16.1 \pm 4.8\%$ versus $10.7 \pm 4.1\%$ shuffled control accuracy; $P < 10^{-12}$; Cohen's $\kappa = 0.06$). Using the direction-dependent reference frame, prediction accuracy was $33.0 \pm 7.6\%$ versus $19.3 \pm 7.2\%$ shuffled control accuracy (Fig. 3b, fourth column; $P = 0.09$ compared to allocentric).

Cross-task generalization of the population code for space. The position of animals in space could be decoded from the population of neurons in each task, but it is not clear whether coding of space generalized across tasks; that is, whether a process of abstraction made the representation of space invariant with respect to the task the animal was engaged in. Although single-neuron spatial coding that is dependent on a variety of behavioral and cognitive factors has been documented in humans, monkeys and rodents, it remains possible that stable spatial encoding in at least a subset of neurons was veridical and task invariant. On the other hand, spatial representations observed in each task could be dependent on encoding of task-related features that were relevant at consistent locations during each task.

To determine whether the cognitive map of space generalized across tasks, we trained a linear support vector machine using trials from the foraging task and tested it using trials from the associative memory task. Classification accuracy when training and testing across tasks fell below the accuracy reported in both foraging and associative memory tasks (Fig. 3, fifth column; $P < 10^{-5}$ and $P < 10^{-17}$, respectively). Results were unchanged when the training and testing sets were swapped. The lack of generalization indicates that the spatial information carried by the population of recorded neurons changes across tasks. Cross-task decoding accuracy was not uniform across all areas of the maze, as can be seen in the cross-task confusion matrix (Fig. 3c, farthest right; Extended Data Fig. 6b; $P < 10^{-5}$, Kruskal–Wallis test). Decoding accuracy was highest in the corridor of the maze (Extended Data Fig. 6b,c; 43%, $P < 10^{-15}$ compared to shuffled control decoding accuracy). This suggests that the contribution of individual neurons to direction-dependent position classification was most similar across tasks in
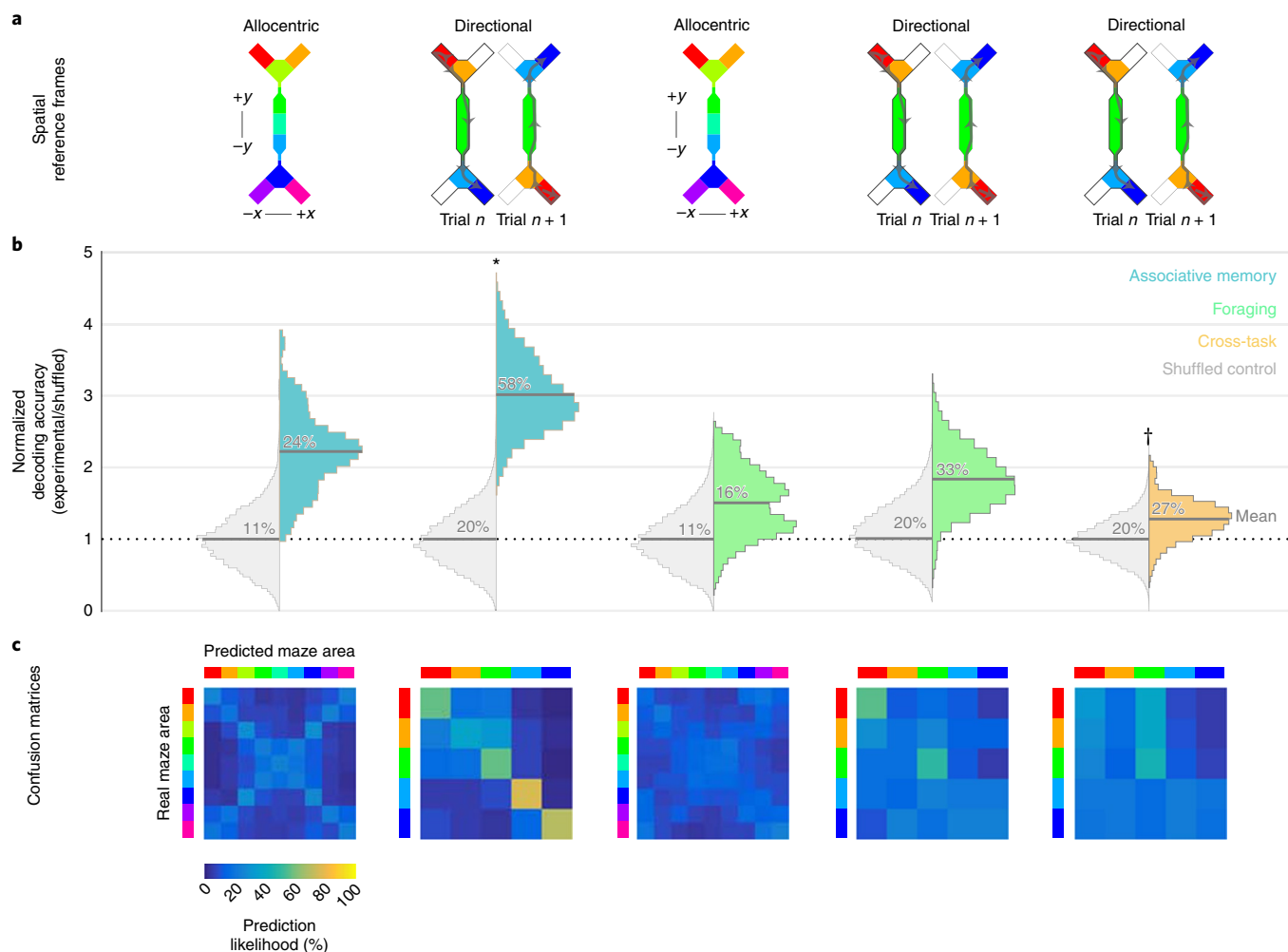
Fig. 3 | Hippocampal ensemble prediction of spatial position with a linear classifier. a, Spatial reference frames used in each of the lower panels of spatial classification analyses. **b,** Distributions of classification accuracies for spatial position in the associative memory (blue) and foraging (green) tasks as well as cross-task testing and validation (orange). Gray bars indicate means. All distributions, $P < 0.05$ real versus shuffled distribution (gray distributions). $n = 50$ per distribution, two-sided Wilcoxon rank-sum test. *$P < 0.05$, allocentric versus directional within task ($n = 50$ per distribution; two-sided Wilcoxon rank-sum test). †$P < 0.05$, cross-task versus associative memory and foraging tasks, directional reference frame ($n = 50$ per distribution; two-sided Wilcoxon rank-sum test). **c,** Confusion matrices for each classification analysis. Real location, rows; predicted location, columns; color map, prediction likelihood.

the corridor. Notably, cross-task demands were also most similar in this area, since only cue-guided wayfinding was required. On the other hand, task requirements were different during the approach to the arms of the maze, where context-dependent choices were required in the associative memory task. In the branch leading toward the arm, and on entry into the arm of the maze, cross-task decoding accuracy was not different from chance (Extended Data Fig. 6c; $P = 0.25$ and $P = 0.85$, respectively). Thus, the population code for space may be the most similar in areas of the maze where task demands are most similar and diverges where task-specific information becomes available.

It is possible that place-specific firing can be ascribed to selectivity for eye-on-screen position[34] coupled with biased gaze behavior within or across tasks. In each session, the X-Maze tasks were bookended by a cued saccade task wherein monkeys were rewarded for making a saccade to a small white dot that varied position from trial to trial on a gray screen. We compared saccade direction and gaze position selectivity in all three tasks for neurons with sufficient numbers of saccades and fixations in all tasks ($n = 92$; see Methods). In the cued saccade, foraging and associative memory tasks, 7.6, 41.3 and 42.4% of neurons were selective for saccade direction,

respectively. In these three tasks, 28.2, 43.4 and 72.8% of neurons were selective for gaze position. Critically, no neurons were selective for the same saccade direction across tasks and only 2 neurons (2.2%) were selective for at least one gaze position across all tasks. Thus, saccade direction and gaze position invariably affect only a small proportion of hippocampal neurons, suggesting that altered fixation patterns across tasks cannot explain the dramatic changes in spatial selectivity across tasks.

Neurons encode nonspatial sensory and mnemonic features of the associative memory task. The previous results show that the population code for space changes across tasks in the areas of the X-Maze where associative memory task features (context, object color and their conjunction) become visible. One possible explanation for this result may be the emergence of selectivity for such features during the associative memory task in single neurons. To examine this, we split each trial into five epochs closely corresponding to the five areas of the maze used in the direction-dependent spatial decoding (postreward, precontext, context appearance, object appearance, object approach; see Fig. 4a and Methods for details). Extended Data Fig. 7 shows the spatial firing distribution
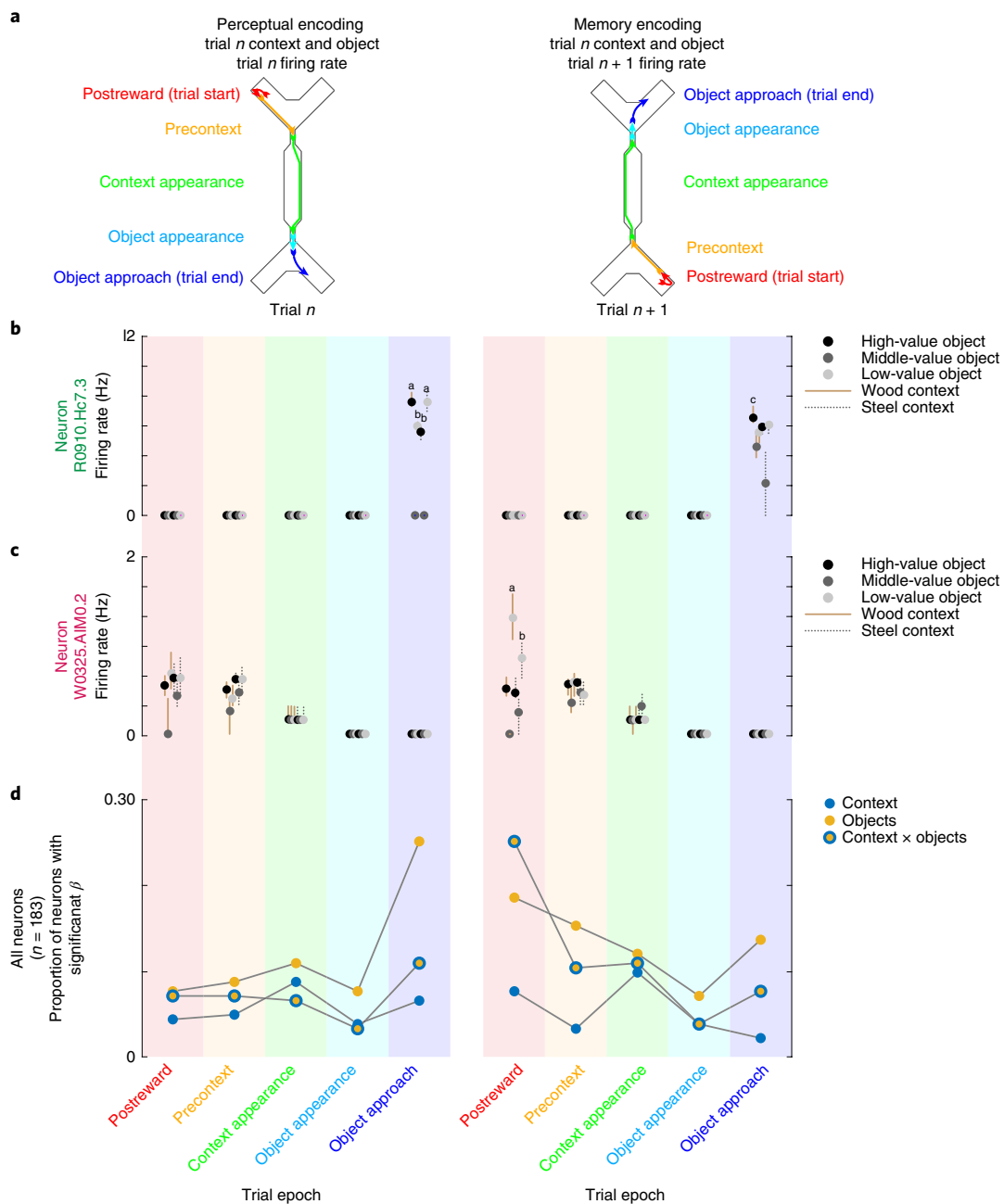
Fig. 4 | Nonspatial feature selectivity in the associative memory task. a, Selectivity of each neuron for nonspatial features of the associative memory task. Selectivity was computed using the trial parameters of trial n and the firing rates from the same trial (perceptual; left plots), or trial $n+1$ (memory; right plots). **b**, Example neuron R0910.Hc7.3, an object-color-selective neuron. The letters denote categories with significantly different firing rates within a trial epoch (two-sided Kruskal–Wallis test, Bonferroni-corrected, $n=296$ trials). The dots indicate the median value; the lines indicate the 25th–75th percentiles. **c**, Example neuron W0325.A1M0.2, an object-value-selective neuron. Conventions are the same as in **b**; $n=257$ trials. **d**, Proportion of single neurons ($n=183$) selective for nonspatial associative memory task features: context (blue dot), chosen object color (yellow dot) and combination of these two (yellow dot, blue outline).

as well as the firing rate in each trial epoch for six example neurons. The firing rate was modulated across associative memory trial epochs for 89.6% of neurons ($P<0.05$, Kruskal–Wallis test).

To determine whether neurons encoded features of the associative memory task that are relevant across the different trial epochs (that is, context, object color and their conjunction), we regressed the firing rate for each neuron against the trial-varying parameters of the associative memory task in each epoch in both a sensory and mnemonic manner. This was done using the context and object of

a given trial and the firing rate in each epoch of the same trial (perceptual encoding; Fig. 4, left plots), or the firing rate in each epoch of the next trial (memory encoding; Fig. 4, right plots).

One example neuron (Fig. 4b and Extended Data Fig. 7b (top left)) fired almost exclusively between the animal's initial turn toward the chosen object and the moment of first contact (goal approach epoch). This neuron was most active during approaches to a single object color regardless of context, egocentric (left versus right) or allocentric (northeast, northwest, southeast or southwest arm)

position, and did not fire when approaching an intermediate value object ($P < 10^{-20}$, Kruskal–Wallis test). This neuron also did not fire on goal approach during foraging (Extended Data Fig. 8a).

Another example neuron (Fig. 4c and Extended Data Fig. 7b (bottom right)) fired most in the arms of the maze after the reward was delivered. This example neuron was selective for previous trial features during the postreward epoch ($P < 10^{-4}$, Kruskal–Wallis test). When this selectivity was observed, the object was no longer present in the environment; thus, encoding of the object by this neuron was mnemonic. This neuron did not consistently fire after the reward during the foraging task (Extended Data Fig. 8b). This encoding cannot be explained by sensory features such as object color, context or reward size alone, but only by the conjunction of these features, even though none of these features were visible during the postreward epoch.

At the population level, sensory coding for the chosen object color was most robust during the object approach epoch (46 out of 183 neurons, 25.14%; Fig. 4d, bottom left, yellow dots). The conjunction of object and context of the previous trial was encoded by the same number of neurons during the postreward epoch (Fig. 4d, bottom right, yellow dots with blue outline). Encoding of trial context peaked in the corridor of the maze (perceptual: 16 out of 183 neurons, 8.7%, memory: 18 out of 183 neurons, 9.8%; Fig. 4d, blue dots). During the object approach and postreward epochs, context selectivity was less prevalent than selectivity for objects and context-object association.

These results show that encoding of nonspatial features changes across trial epochs of the associative memory task, predominantly during the object approach epoch when the animals foveate the objects and context (perceptual encoding), and after the objects are no longer visible (mnemonic encoding). To determine whether perceptual and mnemonic encoding are supported by a common or separate population of hippocampal neurons, we correlated the F-statistics from each neuron's encoding model during goal approach (perceptual) and postreward (memory) epochs. Similar proportions of neurons showed perceptual and mnemonic coding of contexts (Fig. 5a, left, $P = 0.68$, McNemar's test of equal proportions) or objects (Fig. 5a, middle, $P = 0.12$, McNemar's test of equal proportions). However, for the combination of object and context, the proportion of neurons showing memory coding was significantly larger than perceptual coding (Fig. 5a, right, $P = 0.0005$, McNemar's test of proportions). The strength of perceptual versus mnemonic coding in individual neurons was not correlated for trial context (Fig. 5b, Spearman's ρ 95% confidence interval (CI) $= -0.12$ to 0.25); in contrast, perceptual and memory coding for objects and object-context combinations were correlated (Fig. 5b objects: Spearman's ρ 95% CI $= 0.13$–0.48; context×object, 0.05–0.40). This suggested that there was a partial overlap between perceptual and mnemonic information encoded by individual neurons in the associative memory task.

Decoding trial features from the population of hippocampal neurons. We next examined how the recorded hippocampal neurons form a population-level representation of the trial-varying aspects of the associative memory task. We used a linear classifier to determine the accuracy with which the population activity of hippocampal neurons can be used to predict the context and object pair presented in a given trial (associative memory trial type). First, a classifier was trained to predict the context and object of the current trial from the three trial epochs with these visible in the environment (context appearance, object appearance and object approach; Fig. 6, perceptual). Second, another classifier was trained using the two trial epochs that were linked to mnemonic representations of these elements after they were no longer present in the environment (postreward and precontext; Fig. 6, memory). In both classifiers, each neuron's firing rate in each trial epoch was used as an

independent feature; we used a logistic classifier with elastic net regularization to avoid problems of overfitting associated with having many features and a limited number of model training examples (see Methods).

Using only the perceptual or memory epochs, prediction accuracy was above chance (perceptual: $36.3 \pm 14.2\%$ accuracy versus $12.3 \pm 2.7\%$ shuffled control accuracy; $P < 10^{-86}$, Wilcoxon rank-sum test, Cohen's $\kappa = 0.24$; memory: $26.6 \pm 12.5\%$ accuracy versus $12.8 \pm 3.7\%$ shuffled control accuracy; $P < 10^{-58}$, Wilcoxon rank-sum test, Cohen's $\kappa = 0.12$). Using an equal number of trial epochs for training and testing, decoding accuracy was higher for perceptual epochs (object appearance and object approach) than using the two mnemonic trial epochs ($P < 0.001$, Wilcoxon rank-sum test; Extended Data Fig. 9). Using the firing rates from both the perceptual and memory trial epochs in a single classifier, classification accuracy further increased (3.29 ± 1.12 times permuted control; $42.2 \pm 14.4\%$ accuracy; $P < 10^{-97}$, Wilcoxon rank-sum test; Cohen's $\kappa = 0.31$). This is consistent with the observation in Fig. 5 that that perceptual and mnemonic encoding did not fully overlap in individual neurons.

These single-neuron and population-level results provide insights into how the critical elements of associative memories are encoded by hippocampal neurons. All features of a trial that are relevant to the monkeys' decision-making are represented in a proportion of neurons. This representation is sufficient for a 'read-out' mechanism to extract the identity of context and objects from each trial during object viewing and after their disappearance.

Discussion

In the current study, we recorded the activity of individual hippocampal neurons while monkeys performed a foraging and an associative memory task in the same freely navigable maze (Fig. 1). During both tasks, hippocampal neurons encoded spatial information, although single-neuron (Fig. 2) and population-level coding of space changed across tasks (Fig. 3). Critically, observed changes to spatial coding across tasks were attributed to selectivity for trial-varying features of the associative memory task visible in the environment (sensory representation) and when they were no longer visible (mnemonic representation) (Figs. 4 and 5). The population could be used to decode trial types from both the sensory and mnemonic epochs of the associative memory task (Fig. 6). These results extend previous characterizations of hippocampal neurons, showing that encoding of space is nonlinearly mixed with sensory and mnemonic coding of perceptually and cognitively defined features.

Encoding of space in the primate hippocampus. The hippocampus has been referred to as the global positioning system of the brain. This claim is supported by decades of study showing allocentric spatial firing fields of hippocampal place cells in rodents[19]. Place cells are supported by a vast network of neurons in the hippocampus and neighboring brain areas with complementary spatial coding schemes[19,35]. Whether spatial response fields recorded from the hippocampi of primates are like place fields described in rodents has long been subject to debate, in part due to the distinct way experiments are conducted in the different species. Several studies have shown spatial firing fields for neurons recorded from the hippocampi of monkeys performing an operant joystick task that resulted in the movement of a motorized cab around a laboratory[36,37]. However, it is difficult to compare these with rodent studies since movement in these tasks was highly restricted, place fields were defined using a liberal statistical criterion and the confounding effects of view and other task-related factors were not characterized. Similar issues complicate the first studies of hippocampal activity in virtually navigating primates[23]. The first experiments recording animal and gaze position in the environment described spatial view
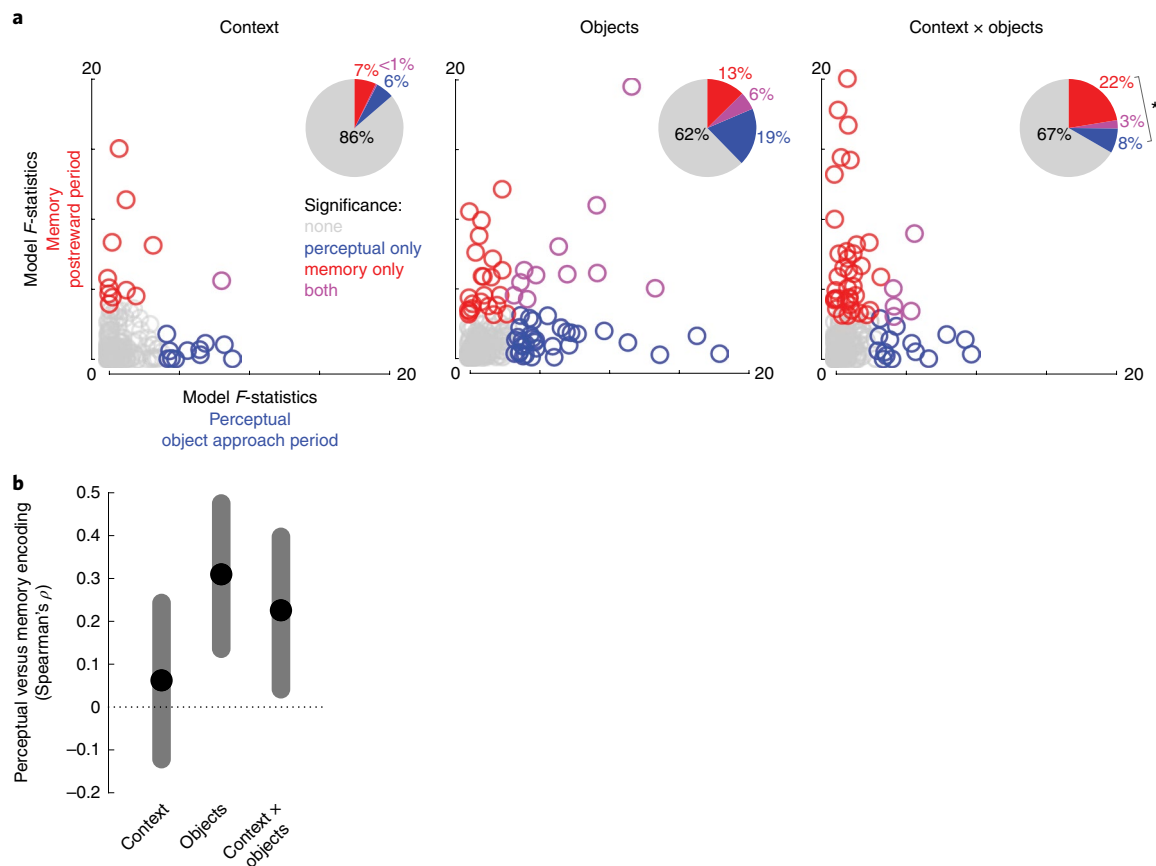
Fig. 5 | Perceptual versus memory encoding of trial features. a, Perceptual versus memory encoding model: fit parameter *F*-statistics comparison. Inset: percentage of neurons with significant fit parameters for each encoding model. **b**, Spearman's correlation coefficient of encoding model *F*-statistics for each neuron between foraging and associative memory tasks (*n* = 183 neurons). Circles, medians; shaded bars, 99% CI.

cells in the hippocampus[20], suggesting that the primate hippocampus encodes a plethora of signals related to vision and the oculomotor system, which are not documented in rodents[9].

Studies of spatial navigation in virtual reality environments have also been conducted in humans. In a study of patients with epilepsy completing a delivery task in a virtual town[21], firing rates of single hippocampal neurons were tested using an analysis of variance for main effects of position within the environment, objects viewed in the environment, navigational goal and interactions. It is possible that trial-varying factors such as goal location could have modulated spatial responses, which is consistent with our findings. A recent study with monkeys performing a virtual wayfinding task has provided a more comprehensive analysis of hippocampal encoding[25]. In this study, 41% of hippocampal neurons had significant SIC. However, only a small percentage of neurons exclusively encoded spatial position, which is consistent with our findings. An extension of this work shows that spatial response fields in a subset of these neurons are invariant to the specific distal landmarks that define an environment[24]. This may suggest that hippocampal neurons form highly task-specific representations of schematic variables in an abstract task space; alternately, they may encode motor or cognitive variables that are common across environments, such as distance to the reward[38]. However, these alternate explanations would not account for task-specific activity observed in the present study (Extended Data Fig. 8) or the selectivity for particular objects and contexts in the associative memory task (Fig. 5).

Our study builds on previous studies of spatial coding in the primate hippocampus by examining single-neuron and population-level codes for a single virtual environment across two tasks.

Our results suggest that neuronal ensembles most reliably encode space in an egocentric direction-dependent reference frame. The magnitude of this effect could be driven by the fact that in our task allocentric cues were not needed to obtain rewards. Spatial representations were task-dependent, in contrast to predictions of a pure spatial role of the hippocampus in navigation[19,35]. Furthermore, task-dependent neuronal activity was attributed to perceptual and mnemonic selectivity for task-relevant features that were observed at varying positions in the environment.

Mixed selectivity for spatial and nonspatial features by single neurons and neuronal ensembles. Spatial and nonspatial encoding have been previously observed in hippocampal neurons across species. The hippocampus has been theorized to encode all aspects of attended experience[39] and it has been suggested that encoding of perceptual content may support recollection through high-resolution associative binding of percepts[40]. In rodents, subsets of hippocampal neurons have been shown to 'map' continuous scalar quantities other than physical space, including time[41] and pitch[42]. In primates, hippocampal neurons show stimulus selectivity in delayed match to sample tasks[12,43]. A recent study that used a cued wayfinding task[25] reported neurons that convey information related to heading direction, gaze position and 'state–space' (combination of these variables and/or recent route and actions). Neurons in the monkey hippocampus can be selective for nonspatial stimuli such as faces and voices[44]. Similarly, selectivity for faces and places is more alike when patients are cued to remember their association[45].

Although a spatial and nonspatial hippocampal activity has been described, it was previously unclear whether changes in spatially
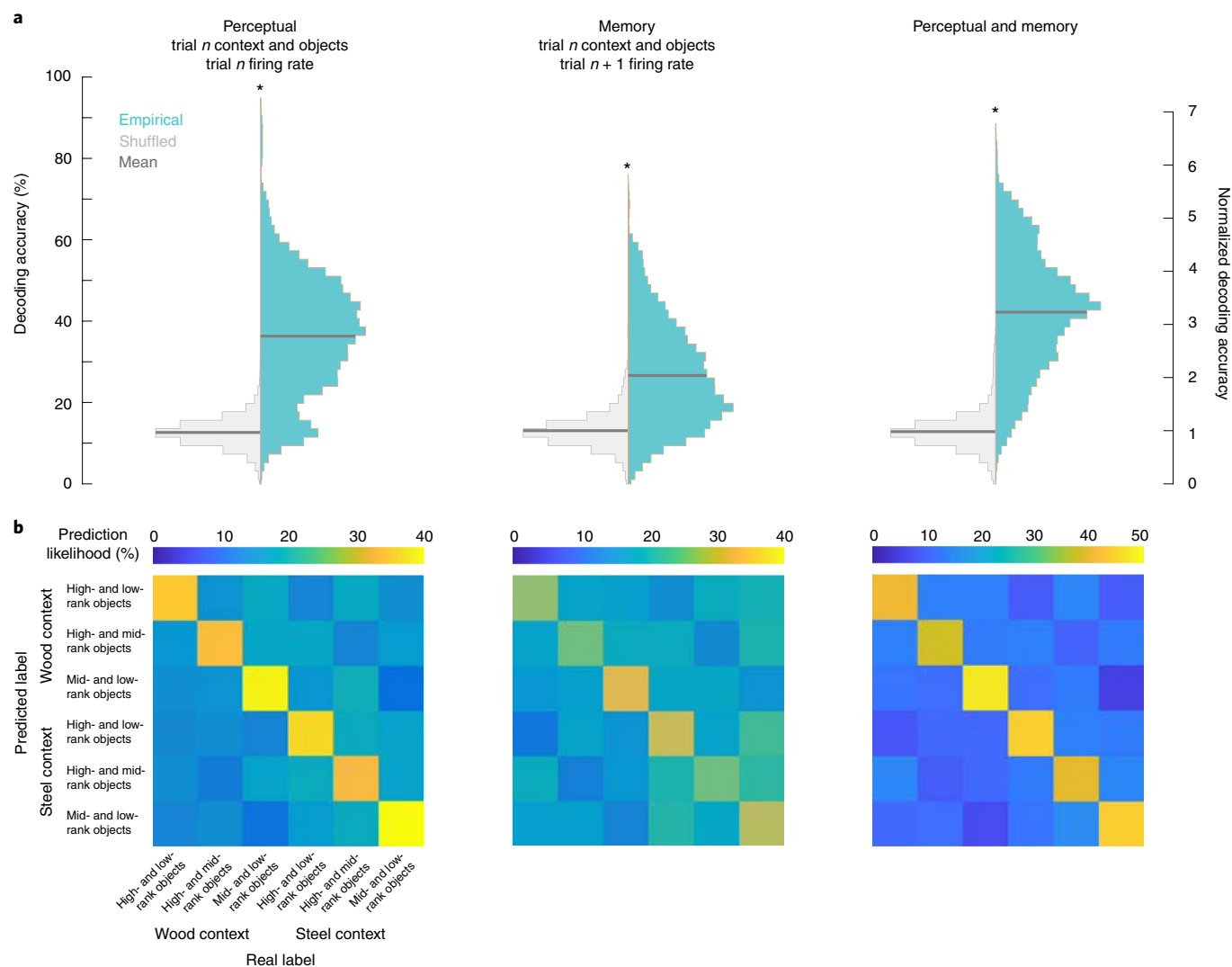
Fig. 6 | Trial type decoding in the associative memory task. a, Distribution of classification accuracies from the decoding analysis of trial type (trial context and object pair) in the associative memory task. Gray bars indicate means. *$P < 0.05$, real (blue) versus shuffled (gray) distribution. $n = 50$ per distribution; two-sided Wilcoxon rank-sum test. **b**, Confusion matrix derived from the classification analysis. Predicted trial type, rows; real trial type, columns; color map, prediction likelihood.

specific firing could be related to associative learning and memory for features of the environment when their spatial position is not relevant. We examined task-specific encoding of trial parameters in the firing rates of hippocampal neurons from the current (perceptual; Fig. 4, trial n) and previous (mnemonic; Fig. 4, trial $n + 1$) trial. Perceptual and mnemonic encoding of trial features were found in separate populations of neurons (Fig. 5). Importantly, the population activity vector could be used to decode single trial-specific feature combinations (Fig. 6).

Mixed coding schemes can be highly robust and computationally efficient[28,46]. In these schemes, selectivity across multiple feature dimensions (for example, space and task-relevant objects) can be mixed in a linearly additive or nonlinearly additive manner. If the spatial and nonspatial coding observed in the present study was linearly additive, the modulation of neural firing rates by nonspatial task-relevant features would be independent of modulation of firing rates by spatial position. However, the single-neuron and population-level representation of space did not generalize across tasks. This suggests that primate hippocampal neurons encode spatial and nonspatial information in a nonlinearly mixed manner.

Sensory information can be compressed using a simple network trained as a sparse autoencoder[47]. The architecture of the hippocampus has long been compared to that of an autoassociative network that is capable of analogous compression of information[48–50]. Mixed coding of spatial and nonspatial components of unfamiliar and familiar episodes may be an emergent consequence of this process; this is consistent with the task-dependent representations of spatial and nonspatial selectivity observed in the present study and elsewhere[5–7]. The distinct coding of these spatial and nonspatial elements of experience across time and space may be viewed as a prerequisite for encoding of episodic memories.

Conclusions
In this study, we sought to reveal how coding of space and nonspatial features interact in the primate hippocampus in virtual environments. Key findings include the encoding of space by single neurons and neuronal populations, as well as the emergence of perceptual and mnemonic codes for nonspatial features in the same populations when the task requirements change but the environment spatial layout is preserved. Instead of framing the primate hippocampus as the brain's global positional system, our results better reflect the

processes inherent in a general abstract processing system that is driven by a broad range of behaviorally relevant inputs. In such a system, flexible representations could provide the basis for learning and storing relevant information unique to an experience across behaviorally relevant dimensions in a context-dependent manner.

Online content

Any methods, additional references, Nature Research reporting summaries, source data, extended data, supplementary information, acknowledgements, peer review information, details of author contributions and competing interests, and statements of code and data availability are available at https://doi.org/10.1038/s41593-019-0548-3.

References

1. Buzsáki, G. & Moser, E. I. Memory, navigation and theta rhythm in the hippocampal–entorhinal system. *Nat. Neurosci.* **16**, 130–138 (2013).
2. Nadel, L. The hippocampus and space revisited. *Hippocampus* **1**, 221–229 (1991).
3. O'Keefe, J. & Nadel, L. *The Hippocampus As a Cognitive Map* (Clarendon Press, 1978).
4. Eichenbaum, H. The role of the hippocampus in navigation is memory. *J. Neurophysiol.* **117**, 1785–1796 (2017).
5. Eichenbaum, H. & Cohen, N. J. Can we reconcile the declarative memory and spatial navigation views on hippocampal function? *Neuron* **83**, 764–770 (2014).
6. Ekstrom, A. D. & Ranganath, C. Space, time, and episodic memory: the hippocampus is all over the cognitive map. *Hippocampus* **28**, 680–687 (2018).
7. Schiller, D. et al. Memory and space: towards an understanding of the cognitive map. *J. Neurosci.* **35**, 13904–13911 (2015).
8. Preuss, T. M. Taking the measure of diversity: comparative alternatives to the model-animal paradigm in cortical neuroscience. *Brain Behav. Evol.* **55**, 287–299 (2000).
9. Rolls, E. T. & Wirth, S. Spatial representations in the primate hippocampus, and their functions in memory and navigation. *Prog. Neurobiol.* **171**, 90–113 (2018).
10. Squire, L. R. Memory and the hippocampus: a synthesis from findings with rats, monkeys, and humans. *Psychol. Rev.* **99**, 195–231 (1992).
11. Jutras, M. J. & Buffalo, E. A. Recognition memory signals in the macaque hippocampus. *Proc. Natl Acad. Sci. USA* **107**, 401–406 (2010).
12. Rolls, E. T. et al. Hippocampal neurons in the monkey with activity related to the place in which a stimulus is shown. *J. Neurosci.* **9**, 1835–1845 (1989).
13. Fried, I., MacDonald, K. A. & Wilson, C. L. Single neuron activity in human hippocampus and amygdala during recognition of faces and objects. *Neuron* **18**, 753–765 (1997).
14. Suthana, N. A. et al. Specific responses of human hippocampal neurons are associated with better memory. *Proc. Natl Acad. Sci. USA* **112**, 10503–10508 (2015).
15. Wirth, S. et al. Single neurons in the monkey hippocampus and learning of new associations. *Science* **300**, 1578–1581 (2003).
16. Rolls, E. T. & Xiang, J.-Z. Reward-spatial view representations and learning in the primate hippocampus. *J. Neurosci.* **25**, 6167–6174 (2005).
17. Wirth, S. et al. Trial outcome and associative learning signals in the monkey hippocampus. *Neuron* **61**, 930–940 (2009).
18. O'Keefe, J. & Dostrovsky, J. The hippocampus as a spatial map. Preliminary evidence from unit activity in the freely-moving rat. *Brain Res.* **34**, 171–175 (1971).
19. Moser, E. I., Moser, M.-B. & McNaughton, B. L. Spatial representation in the hippocampal formation: a history. *Nat. Neurosci.* **20**, 1448–1464 (2017).
20. Rolls, E. T. & Xiang, J. Z. Spatial view cells in the primate hippocampus and memory recall. *Rev. Neurosci.* **17**, 175–200 (2006).
21. Ekstrom, A. D. et al. Cellular networks underlying human spatial navigation. *Nature* **425**, 184–188 (2003).
22. Miller, J. F. et al. Neural activity in human hippocampal formation reveals the spatial context of retrieved memories. *Science* **342**, 1111–1114 (2013).
23. Hori, E. et al. Place-related neural responses in the monkey hippocampal formation in a virtual space. *Hippocampus* **15**, 991–996 (2005).

24. Baraduc, P., Duhamel, J. R. & Wirth, S. Schema cells in the macaque hippocampus. *Science* **363**, 635–639 (2019).
25. Wirth, S., Baraduc, P., Planté, A., Pinède, S. & Duhamel, J.-R. Gaze-informed, task-situated representation of space in primate hippocampus during virtual navigation. *PLoS Biol.* **15**, e2001045 (2017).
26. Averbeck, B. B. & Lee, D. Effects of noise correlations on information encoding and decoding. *J. Neurophysiol.* **95**, 3633–3644 (2006).
27. Rigotti, M. et al. The importance of mixed selectivity in complex cognitive tasks. *Nature* **497**, 585–590 (2013).
28. Fusi, S., Miller, E. K. & Rigotti, M. Why neurons mix: high dimensionality for higher cognition. *Curr. Opin. Neurobiol.* **37**, 66–74 (2016).
29. Doucet, G., Gulli, R. A. & Martinez-Trujillo, J. C. Cross-species 3D virtual reality toolbox for visual and cognitive experiments. *J. Neurosci. Methods* **266**, 84–93 (2016).
30. Markus, E. J., Barnes, C. A., McNaughton, B. L., Gladden, V. L. & Skaggs, W. E. Spatial information content and reliability of hippocampal CA1 neurons: effects of visual input. *Hippocampus* **4**, 410–421 (1994).
31. Skaggs, W. E., McNaughton, B. L., Gothard, K. M. & Markus, E. J. An information-theoretic approach to deciphering the hippocampal code. In *Proc. Advances in Neural Information Processing Systems 5* (eds Hanson, S. J. et al.) 1030–1037 (Morgan Kaufmann Publishers, 1993).
32. Treves, A. & Panzeri, S. The upward bias in measures of information derived from limited data samples. *Neural Comput.* **7**, 399–407 (1995).
33. Acharya, L., Aghajan, Z. M., Vuong, C., Moore, J. J. & Mehta, M. R. Causal influence of visual cues on hippocampal directional selectivity. *Cell* **164**, 197–207 (2016).
34. Killian, N. J., Jutras, M. J. & Buffalo, E. A. A map of visual space in the primate entorhinal cortex. *Nature* **491**, 761–764 (2012).
35. Hartley, T., Lever, C., Burgess, N. & O'Keefe, J. Space in the brain: how the hippocampal formation supports spatial cognition. *Philos. Trans. R. Soc. Lond. B* **369**, 20120510 (2014).
36. Matsumura, N. et al. Spatial- and task-dependent neuronal responses during real and virtual translocation in the monkey hippocampal formation. *J. Neurosci.* **19**, 2381–2393 (1999).
37. Ono, T., Nakamura, K., Nishijo, H. & Eifuku, S. Monkey hippocampal neurons related to spatial and nonspatial functions. *J. Neurophysiol.* **70**, 1516–1529 (1993).
38. Gauthier, J. L. & Tank, D. W. A dedicated population for reward coding in the hippocampus. *Neuron* **99**, 179–193.e7 (2018).
39. Morris, R. G. M. & Frey, U. Hippocampal synaptic plasticity: role in spatial learning or the automatic recording of attended experience? *Philos. Trans. R. Soc. Lond. B* **352**, 1489–1503 (1997).
40. Yonelinas, A. P. The hippocampus supports high-resolution binding in the service of perception, working memory and long-term memory. *Behav. Brain Res.* **254**, 34–44 (2013).
41. Kraus, B. J., Robinson, R. J.2nd, White, J. A., Eichenbaum, H. & Hasselmo, M. E. Hippocampal 'time cells': time versus path integration. *Neuron* **78**, 1090–1101 (2013).
42. Aronov, D., Nevers, R. & Tank, D. W. Mapping of a non-spatial dimension by the hippocampal–entorhinal circuit. *Nature* **543**, 719–722 (2017).
43. Colombo, M., Fernandez, T., Nakamura, K. & Gross, C. G. Functional differentiation along the anterior-posterior axis of the hippocampus in monkeys. *J. Neurophysiol.* **80**, 1002–1005 (1998).
44. Sliwa, J., Planté, A., Duhamel, J.-R. & Wirth, S. Independent neuronal representation of facial and vocal identity in the monkey hippocampus and inferotemporal cortex. *Cereb. Cortex* **26**, 950–966 (2016).
45. Ison, M. J., Quian Quiroga, R. & Fried, I. Rapid encoding of new memories by individual neurons in the human brain. *Neuron* **87**, 220–230 (2015).
46. Johnston, W. J., Palmer, S. E. & Freedman, D. J. Nonlinear mixed selectivity supports reliable neural computation. Preprint at *bioRxiv* https://www.biorxiv.org/content/biorxiv/early/2019/03/14/577288.full.pdf (2019).
47. Olshausen, B. A. & Field, D. J. Sparse coding with an overcomplete basis set: a strategy employed by V1? *Vision Res.* **37**, 3311–3325 (1997).
48. Marr, D. Simple memory: a theory for archicortex. *Philos. Trans. R. Soc. Lond. B* **262**, 23–81 (1971).
49. Tank, D. W. & Hopfield, J. J. Collective computation in neuronlike circuits. *Sci. Am.* **257**, 104–114 (1987).
50. Benna, M. K. & Fusi, S. Are place cells just memory cells? Memory compression leads to spatial tuning and history dependence. Preprint at *bioRxiv* https://www.biorxiv.org/content/biorxiv/early/2019/04/30/624239.full.pdf (2019).

Methods

Experimental animals. Two rhesus macaques (*Macaca mulatta*; 7 years old, 7 kg and 14 years old, 12 kg) participated in all experiments. These monkeys were trained to perform three behavioral tasks and given a juice reward for their efforts in each task (400–1,000 ml daily). Monkeys also received food rewards as positive reinforcement at the beginning and end of each session. Behavioral patterns and body weights were closely monitored to ensure stable health conditions throughout the experiment. All animal procedures complied with the Canadian Council on Animal Care guidelines and were approved by the McGill University Animal Care Committee.

Electrophysiological recordings. The entire protocol for planning the surgical procedures, recording from the hippocampus and verifying electrode locations is schematized in Extended Data Fig. 1.

Before any surgical procedures, a naïve 500 μm isotropic T1-weighted 3-Tesla MRI was taken for each animal (Extended Data Fig. 1, step 1). Using these scans, head post placement and chamber trajectory were planned using an MRI-guided neuronavigation suite (Brainsight TMS; Rogue Research; Extended Data Fig. 1, step 2). Chambers were positioned over the prefrontal cortex, such that electrode trajectories were perpendicular to the long and transverse axis of the right middle-to-posterior hippocampus. Following surgical implantation of the head post and recording chamber, a computed tomography scan was acquired with cannulas passing through the chamber grid at cardinal locations (Extended Data Fig. 1, step 3). The resultant computed tomography and MRI scans were co-registered so that electrode trajectories and terminal recording locations could be specifically mapped to chamber grid holes (Extended Data Fig. 1, step 4).

All data were collected over the course of 37 recording sessions. In each session, hippocampal activity was recorded using up to 4 single high-impedance tungsten electrodes (0.4–1.5 MOhms) simultaneously. Before every recording session, electrode trajectories were mapped to the MRI and the expected distances to gray and white matter were measured (Extended Data Fig. 1, step 5). These expected waypoints were compared against changes in neural activity while the electrode was lowered to the terminal recording site (speed 0.01 mm s⁻¹; Extended Data Fig. 1, step 6). Distances to putative CA3 recording sites were adjusted online as necessary.

Neurons from the hippocampus were isolated while animals sat quietly in the dark recording room since hippocampal neurons typically exhibit elevated firing rates in this state compared to foraging or other exploratory behaviors. Local field potentials were monitored for bouts of theta-like activity and changing low-frequency power profile as a function of arousal. Multiunit activity was monitored for sparse activity and burstiness characteristic of hippocampal pyramidal neurons. Hippocampal activity was recorded at 30,000 Hz using a multichannel recording system (128-channel Cerebus Data Acquisition System; Blackrock Microsystems) for sorting and offline analysis. Cluster cutting to isolate neurons from multiunit clusters was done using Plexon software (Offline Sorter version 2.8.8; Plexon Inc). Cluster cutting was done agnostic to time; however, neurons with continuously morphing principal components and/or a complete loss of activity as a function of time were excluded from the analyses. Any neurons with task-invariant, reward-related activity were excluded from the analyses.

In one monkey, postrecording verification of electrode trajectories was possible. This was done using a 350 μm isotropic susceptibility weighted 7-Tesla MRI (Extended Data Fig. 1, step 7, cool color map). This scan was co-registered to the naïve 3-Tesla anatomical MRI and shows a high degree of concordance between expected and actual trajectories and terminal recording locations.

Experimental setup. During the training and experimental sessions, the monkeys were seated in a custom-built chair in front of a computer monitor. The chair was fitted with a two-axis joystick (part no. 212S15S8383; P-Q Controls), which the monkeys used to navigate freely through the virtual environment. Player position within the virtual environment was updated and recorded at 75 Hz, which matched the monitor refresh rate. While seated, the head position of the monkey was fixed to facilitate eye position and intrahippocampal recordings. Eye position on the screen—and thus gaze within the virtual environment—was monitored at 500 Hz via video-based eye tracking (EyeLink 1000; SR Research).

Behavioral tasks. After electrode positions were fine-tuned to optimize neuronal signal-to-noise ratios, monkeys typically sat quietly in the darkened room for 20 min, allowing sufficient time for electrodes to settle. After this, monkeys proceeded to complete three behavioral tasks: a cued saccade task; a virtual associative memory task; and a virtual foraging task. At the end of each session, the cued saccade task was repeated and monkeys again sat quietly in the dark for an additional 10–20 min of recording.

In the cued saccade task, monkeys were trained simply to fixate on a 1 degree visual angle white dot that could appear at any of 9 locations on the monitor in a 24 × 16 degree visual angle grid.

The remaining two tasks were incorporated into a virtual environment custom-built using a video game engine (Unreal Engine May 2012 release; Epic Games) and parameters of the behavioral tasks could be monitored and controlled in real-time via MATLAB (MathWorks)[29]. Monkeys were trained to freely navigate around

this environment called the X-Maze using a two-axis joystick. Monkeys completed both virtual reality tasks in all experimental sessions in a blocked design (Extended Data Fig. 2). Sessions where only one of the virtual reality tasks was completed were removed from the analyses.

In the virtual foraging task, animals were visually cued to navigate toward an easily identifiable target (red fog) that was consistently rewarded. The target could appear at any of 84 locations in the environment (Fig. 1c, foraging task; 84 dotted locations for display purposes only). Target locations in the X-Maze were independent across trials.

In the associative memory task, monkeys navigated the X-Maze to learn a context-dependent reward value hierarchy. Reward value associations were dependent on environmental cues (textures applied to the maze walls; context 1 and context 2) and three differentially rewarded colored disks (objects A, B and C). Object reward values were context-dependent, that is, in context 1, object A>B>C, and in context 2, object C>B>A (Fig. 1c and Extended Data Fig. 3A). Object colors were pseudorandomly selected from a seven-color set at the beginning of each session to prevent repetition of colors across neighboring sessions. Thus, a new context-object hierarchy was learned every day.

On a single trial, animals started at either the north or south end of the X-Maze. They then navigated through a long central corridor toward the opposite end of the maze. One of two possible textures (wood or steel) was applied to some of the walls of the maze when the monkey reached the corridor (Extended Data Fig. 3b,c, position a). At the end of the corridor, animals reached a forked decision point with each of the two arms containing one of the three possible colored objects (Extended Data Fig. 3b,c, position b).

On individual trials, the context was randomized independently, as was the object-color combination. Object colors were randomly assigned to either the left or right arm of the maze; the same two colors could not appear in each arm of the maze on a single trial.

The quantities of juice reward given for successful completion were fixed between the cued saccade, foraging and middle reward value of the associative memory tasks.

Eye movement classification. We used a custom toolbox to parse the eye signal collected via video-oculography into saccades, fixations, smooth pursuits and postsaccadic oscillations[51]. Briefly, the initial identification of putative saccades was done by: (1) iteratively calculating a saccade acceleration threshold; (2) grouping threshold crossings within 40 ms into a putative saccade; and (3) ignoring putative saccade groups shorter than 10 ms. The remaining segments of the eye signal were further classified by foveation type.

For all putative saccadic periods, the maximum velocity was calculated; then, the onset and offset were identified precisely by comparing the main direction and intersample changes in direction. Saccade boundaries were defined when the signal was either above a high threshold (60°) for 1 sample, or above a low threshold for 3 consecutive samples (20°). This method differentiates between eye movement types since saccade direction is very consistent, whereas camera noise leads to higher intersample variance during smooth pursuits and fixations. Once saccades were identified, direction and amplitude were calculated based on the onset and offset points for all saccades during the visually guided task, including intertrial intervals, and for all completed trials in both virtual navigation tasks. These saccades were used for the analyses of saccade direction selectivity. Saccade offset locations were used to analyze gaze position selectivity on the screen.

Quantification and statistical analyses. *Statistics.* For each analysis, the exact statistical test used is described in the following sections. In general, permutation tests were used for single-neuron analyses of SIC, spatial response fields, saccade direction selectivity and gaze position selectivity. Each neuron's selectivity for features of the associative memory task was assessed using multiple linear regression in conjunction with parametric tests of significance that rely on *F*-statistics to assess significance of individual coefficients. Distributions of decoding accuracies were compared using Wilcoxon rank-sum tests and further examined using Cohen's κ statistic. No statistical methods were used to predetermine sample sizes but our sample sizes are similar to those reported previously[15]. As stated previously, goal location in the cued saccade and foraging tasks were randomized on every trial. In the associative memory task, objects and context were randomized independently on every trial. Data collection and analysis were not performed blind to the conditions of the experiments. Additional information related to the Methods can be found in the Life Sciences Reporting Summary.

Learning analyses. To demonstrate that monkeys learned the importance of context in guiding behavior in the associative memory task, we used a state–space analysis to estimate the learning state based on previous and future trial outcomes from the perspective of an ideal observer to estimate a hidden variable[52]. This produces an estimate of the latent learning state, as well as a 95% confidence interval of the learning state. Extended Data Fig. 3d shows the average learning state, as well as the average bounds for the 95% confidence interval for high-low trials across all sessions. Learning is said to have occurred when the lower 95% confidence interval of the estimated learning state exceeds 50% (refs. [15,52]).

Spatial response fields. To determine whether each neuron fired more action potentials than expected by chance in any area of the X-Maze in each task, we used a statistical permutation test based on spatial position and spike rasters for each neuron (Fig. 2 and Extended Data Fig. 5). First, the X-Maze was parsed into a 32×12 pixel grid. For each trial, a vector of player positions (occupied pixel number) was created at 1 ms resolution. For each recorded neuron, a corresponding binary vector was produced with 1 ms resolution, denoting the presence or absence of an action potential. By collapsing across trials, the occupied time and number of recorded action potentials were computed. To determine if this number was significantly above chance for each pixel, the vector of occupied pixels was circularly shifted for each trial and the firing rate in each pixel was recomputed. This circular shuffling procedure was done 1,000 times. Any pixel with an empirical firing rate exceeding percentile 1-α was statistically significant, where $\alpha = 0.05$/total number of occupied bins. Pixels with a total occupancy of less than 200 ms were excluded. Spatial response fields were defined as any of the 9 architecturally distinct maze areas (4 arms, 2 branches, 3 corridor sections; see Fig. 2, Extended Data Fig. 5 and Fig. 2 (allocentric reference frame)) with at least one statistically elevated spatial bin.

The specificity of each neuron's spatial response map was quantified using the SIC[31,53] (Fig. 1e). Each neuron's information content (L; in bits) is defined as

$$\bar{\lambda} = \sum_{i}^{L} P_i \lambda_i$$

where L is the total number of pixels and the proportion of occupied time (o) in the ith pixel ($_{P_i}$) is defined as

$$P_i = \frac{o_i}{\sum_{j=1}^{L} o_j}$$

and the average firing rate per pixel $\bar{\lambda}$ is $\bar{\lambda} = \sum_{i}^{L} P_i \lambda_i$.

SIC was computed for each neuron for each pixel occupied for more than 200 ms. A null distribution of SIC (and corresponding null spatial information maps) was computed for each neuron by circularly shifting the vector of occupied pixel numbers 1,000 times before computing the spike rate maps for that neuron. Neurons with summed SIC exceeding the 95th percentile of the null distribution were deemed statistically significant. The mean SIC from the shuffled null distribution for each neuron was subtracted from the empirical SIC value for that neuron, yielding a normalized SIC value for each neuron. These normalized SIC values are shown in the cumulative distribution plot in Fig. 1e.

For visualization, conventional firing rate maps (Extended Data Fig. 4) were plotted for the example neurons in Fig. 1d. In these maps, the pixel-wise firing rates were smoothed with a 3-bin Gaussian kernel[41]. Color maps were consistent within neuron and across tasks, with the maximum and minimum firing rates denoted separately for each neuron. The color map was perceptually nonlinear and unordered (jet), consistent with previously published work[54].

Spatial classification analyses. We used a linear support vector classifier[55] to determine whether the population of all recorded neurons could reliably encode position in the maze (Fig. 2). The same procedures were used for all spatial classification analyses, starting with firing rates for all neurons in all trials and respective conditions. 'Trials' here refers to passes through each area of the X-Maze. All neurons that did not have at least 10 trials in all areas were excluded from all classification analyses ($n = 152$ included). To begin, we randomly subsampled ten trials from each condition for each neuron, creating an ensemble subsample. For subsequent classification, we used a linear kernel support vector machine, cross-validated with stratified k-folds. Specifically, we split the ensemble subsample into five stratified groups of trials (five folds), with four folds constituting the training set and one fold reserved for testing. At this point, the firing rate of each neuron in all k-folds was z-scored using the mean and s.d. of the training set only for that neuron (not the testing set). A linear kernel model was fitted to the ensemble subsample using L1-regularized L2-loss support vector classification. An important benefit of using L1 regularization is automatic parameter selection on the model inputs; whereas L2 regularization yields parameter weights very close to zero, L1 regularization instead shunts weights directly to zero. This results in a trained model that is both sparse and more interpretable. The trained model was subsequently tested on the reserved testing fold to assess prediction accuracy. The procedure for normalization, model training and testing was repeated five times in total, so each k-fold of the ensemble subsample was used as the testing set once. The entire procedure—starting from the 10-trial ensemble subsampling—was repeated 100 times, yielding a total of 500 iterations of the support vector machine testing procedure.

A permutation procedure was used to determine chance prediction accuracy in all cases. This proceeded similarly to the training and testing procedures described earlier. However, after creating the ensemble subsample and before splitting the ensemble subsample into stratified k-folds, the condition labels were randomly permuted and classification analyses then proceeded exactly as described previously. This procedure was repeated 20 times for each ensemble subsample, yielding a total of 10,000 individual iterations of the support vector machine testing procedure.

It is important to note that each neuron's firing rate was z-scored in the training set only and within each task independently before classification. This negates the possibility of spurious similarity of cross-task classification models attributed to within-neuron similarity in baseline firing rates across tasks, independent of area-specific changes in firing rate. Similarly, this negates the possibility of spurious dissimilarity of cross-task classification models attributed to within-neuron changes in baseline firing rates across tasks, independent of area-specific changes in firing rate.

Saccade direction selectivity. To examine saccade direction selectivity, we binned directions in eight 45° bins, starting with a center on 0°. A bin was only analyzed if there were at least seven saccades in it; a neuron's saccade direction selectivity was only analyzed with a minimum of five saccade direction bins. The firing rate was calculated for the 150 ms before saccade onset to get the average spike rate for each direction.

Significant direction selectivity for each neuron was assessed using a permutation test. Firing rates and directions were randomly shuffled 1,000 times, generating 1,000 null distributions for each saccade direction for each neuron. A neuron was categorized as being selective for a direction if it had a spike rate that was in the top 5th percentile of the null distribution after Bonferroni correction ($\alpha = 0.05$/number of direction bins).

Gaze position selectivity. Each on-screen foveation was categorized within one of nine 12°×8° screen areas. For each foveation within each screen location, a neuron's firing rate was calculated in the 200 ms after saccade offset. For a location to be included, at least seven saccades in that location were needed. Foveation location selectivity was tested in each task for all neurons, with enough foveations in at least six screen locations in each task. Like saccade direction selectivity, gaze position selectivity of each neuron was assessed using a permutation-derived null distribution.

Nonspatial feature selectivity. For two example neurons, we determined whether firing rate varied in each trial epoch as a function of nonspatial trial features (chosen object color, trial context and their conjunction) from the current and previous trial (Fig. 5a). Key trial events delineated trial epochs. The postreward and precontext epochs were equally split intervals of time between the start of the current trial (approximately 200 ms after reward from the previous trial ended) and the first frame where the context material was applied to the walls of the central corridor. The context appearance epoch started at this frame and extended for the entire path of the animal through the corridor. On reaching the end of the corridor, the animal's view in the maze was gently corrected to face cardinal direction north or south precisely; subsequently, both objects were triggered to appear simultaneously at the ends of the maze. The frame where the objects were first visible marked the end of the context appearance epoch and the start of the object appearance epoch. Animals were free to take as long as needed to make a decision to navigate to the left or right object. The first frame at which the animal's orientation deviated from the cardinal north or south direction, as part of a rotation that eventually exceeded 10° of deviation from midline, marked the end of the object appearance epoch and the start of the object approach epoch. The object approach epoch ended when the animal first touched the chosen object for that trial. Note that the next trial's postreward epoch started approximately 200 ms after the end of the reward delivery.

We used multiple linear regression to determine whether each neuron's firing rate was modulated as a function of nonspatial trial features (that is, trial context, trial object colors and their conjunction) in each trial epoch of the associative memory task. This procedure was repeated using trial features for the current and previous trial. Formally,

$$y_{ij} = \beta_{0ij} + \beta_{1ij} x_{1ij} + \beta_{2ij} x_{2ij} + \beta_{3ij} x_{3ij} + \varepsilon_{ij}$$

where y describes the change in a neuron's firing rate within each task epoch (i; 1, postreward epoch; 2, precontext; 3, context appearance; 4, object appearance; 5, object approach) for current and previous trial features (j; 1, current trial features; 2, previous trial features). Fit parameter β_0 describes the intercept of the regression line, ε estimates the residual, and β_1, β_2 and β_3 describe the effect of chosen object, trial context and their conjunction, respectively. We assessed the statistical significance of each of these parameters using a partial F-test, wherein the error of the full model is compared to that of a model with one parameter omitted. The proportion of all neurons ($n = 183$) with significant fit parameters for object, context or their interaction is reported in Fig. 4c. Data distribution was assumed to be normal but this was not formally tested.

Sensory versus mnemonic trial feature encoding. The F-statistics of the fit parameters β_1, β_2 and β_3 were used to compare sensory and mnemonic encoding of associative memory trial features in individual neurons. Specifically, Fig. 6a shows the scatterplot of the regression coefficients of neurons during the goal approach epoch (sensory encoding) versus the postreward epoch (memory encoding).

The proportion of neurons with significant regression coefficients for each parameter was compared using the McNemar's test of proportions (Fig. 5a, insets).

The relationship between sensory and memory encoding for each trial parameter for each neuron was characterized using Pearson's ρ (Fig. 5b). The value of ρ was calculated over 10,000 bootstrap iterations; Fig. 5b shows the median and 96.7% confidence interval ($\alpha = 0.05$/number of trial parameters).

Trial type classification. Trial type classification (Fig. 6) was done using the Glmnet package[56] using firing rates from all neurons included in the spatial decoding analyses ($n = 152$). For the perceptual condition, each neuron's firing rate from the corridor, goal appearance and goal approach epochs were included as predictors. For the memory condition, firing rates from the postreward and precontext epochs were used as predictors. In the sensory + memory condition, all five epochs were used. Because of the high ratio of model predictors to training and testing examples for these analyses, Glmnet classification was used with elastic net regularization. A nested cross-validation procedure was used to appropriately tune the model hyperparameters (regularization parameter λ and elastic net L1–L2 weighting parameter α via Grid Search) and test on hold-out sets of trials never seen by the trained model.

Statistical evaluation of classifier performance. The mean and s.d. classification accuracy reported in this study includes testing of each individual k-fold. Statistical comparisons of classification accuracy were run using normalized accuracy distributions, wherein the distribution of empirical accuracy values for a condition was divided by the mean accuracy of the shuffled control values for that condition. Significant differences between normalized accuracy for two conditions were tested using a two-sided Wilcoxon rank-sum test, Bonferroni-corrected for the total number of distribution comparisons.

Classification model reliability was further evaluated using Cohen's κ (ref. [57]); κ is an objective measure of classification reliability. Unlike raw or chance-normalized prediction accuracy, κ provides a meaningful metric with which to compare performance across classifiers—even with uncommon numbers of classes—because it is a bound statistic that relies on the observed and expected proportions of correct predictions for each class of a model; it is agnostic to the number of classes being differentiated. It is described as

$$\kappa = \frac{p_o - p_e}{1 - p_e}$$

where p_o is the proportion of correct predictions and p_e is the probability of guessing the correct class by chance.

Reporting Summary. Further information on research design is available in the Nature Research Reporting Summary linked to this article.

Data availability

Data can be downloaded at https://robertogulli.com/data. Further information and requests for resources and protocols should be directed to and will be fulfilled by the lead contact, R.A.G.

Code availability

The code used in the study is available upon request from R.A.G.

References

51. Corrigan, B. W., Gulli, R. A., Doucet, G. & Martinez-Trujillo, J. C. Characterizing eye movement behaviors and kinematics of non-human primates during virtual navigation tasks. *J. Vis.* **17**, 15 (2017).
52. Smith, A. C. et al. Dynamic analysis of learning in behavioral experiments. *J. Neurosci.* **24**, 447–461 (2004).
53. Ravassard, P. et al. Multisensory control of hippocampal spatiotemporal selectivity. *Science* **340**, 1342–1346 (2013).
54. Chen, G., King, J. A., Burgess, N. & O'Keefe, J. How vision and movement combine in the hippocampal place code. *Proc. Natl Acad. Sci. USA* **110**, 378–383 (2013).
55. Fan, R.-E., Chang, K.-W., Hsieh, C.-J., Wang, X.-R. & Lin, C.-J. LIBLINEAR: a library for large linear classification. *J. Mach. Learn. Res.* **9**, 1871–1874 (2008).
56. Friedman, J., Hastie, T. & Tibshirani, R. Regularization paths for generalized linear models via coordinate descent. *J. Stat. Softw.* **33**, 1–22 (2010).
57. Cohen, J. A coefficient of agreement for nominal scales. *Educ. Psychol. Meas.* **20**, 37–46 (1960).

Author contributions

R.A.G. designed the experiments and virtual environments, collected and analyzed the data, and wrote the manuscript. L.R.D. contributed to the data analysis. B.W.C. contributed to data collection and data analysis. G.D. contributed to virtual environment design and data analysis. S.W. contributed to the experimental design. S.F. contributed to data analysis and manuscript writing. J.M.-T. contributed to the experimental design and manuscript writing.

Competing interests

The authors declare no competing interests.

Additional information

Extended data is available for this paper at https://doi.org/10.1038/s41593-019-0548-3.

Supplementary information is available for this paper at https://doi.org/10.1038/s41593-019-0548-3.

Correspondence and requests for materials should be addressed to R.A.G. or J.C.M.-T.
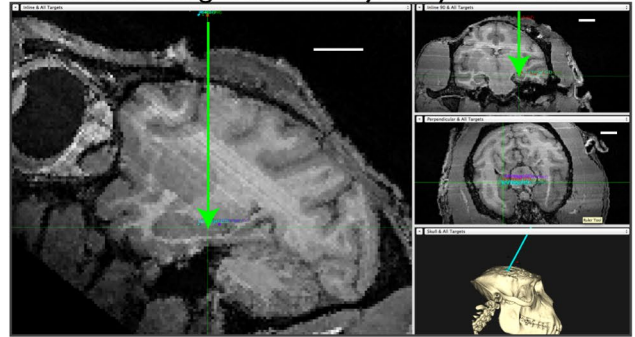
Peer review information *Nature Neuroscience* thanks Arne Ekstrom and the other, anonymous, reviewer(s) for their contribution to the peer review of this work.

Reprints and permissions information is available at www.nature.com/reprints.
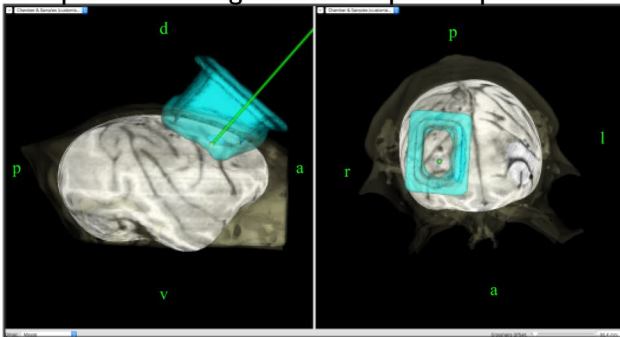
1. MRI on naive monkey
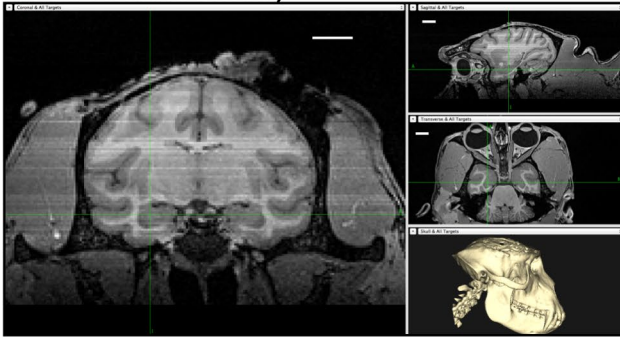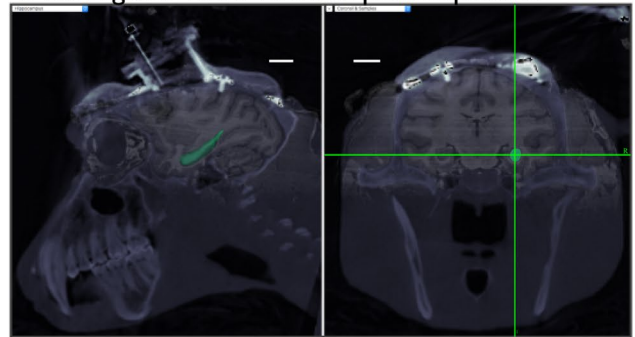
2. Plan recording chamber trajectory towards ROI

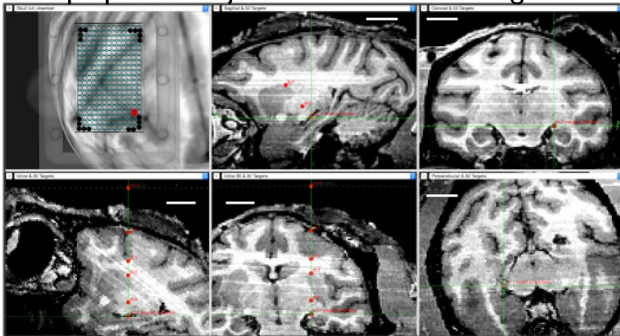3. Implant recording chamber & post-implant CT
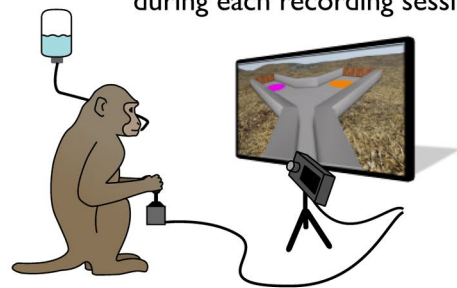
4. Co-register naive MRI and post-implant CT

Volumetric hippocampus reconstruction   Post-implant CT   Naive MRI
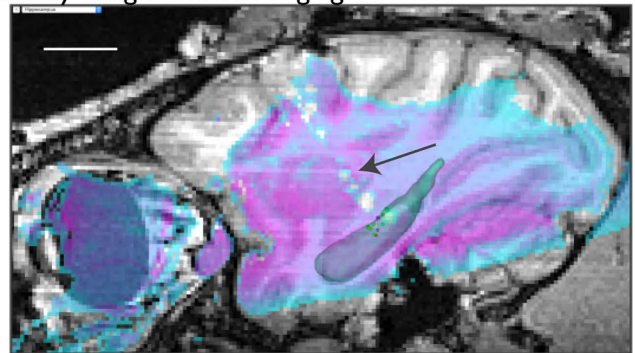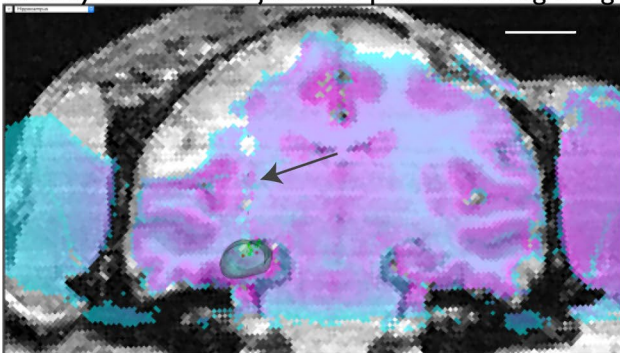
5. Map updated trajectories to hc recording sites offline

6. Verify electrode trajectory mapping online during each recording session

7. Verify electrode trajectories post-recording using susceptibility-weighted MRI imaging

Volumetric hippocampus reconstruction   Naive MRI

Post-recording MRI   Electrode tracts

**Extended Data Fig. 1 | See next page for caption.**

Extended Data Fig. 1 | Hippocampal recordings: planning, mapping and verification. Schematic representation of the major steps in planning, mapping, and verification of electrode trajectories and recording sites. In all cases, scale bars represent 10 mm. 1. Prior to any surgical procedures, a 3T MRI was taken of the naiive monkey. 2. Using Brainsight (Rogue Research, Montreal, Canada), the chamber trajectory was planned. The skull was then 3D-printed, and a mock surgical procedure was done to recreate the chamber trajectory. A custom-made footed chamber was then formed to the skull at its intended placement with the intended trajectory. 3. A titanium (monkey R) or silex (monkey W) chamber was implanted along the planned trajectory. Subsequently, a post-implant computed tomography scan was taken with the recording grid and electrodes in place in order to visualize the electrode trajectories. 4. The computed tomography scan was co-registered to the naiive MRI. 5. The updated trajectory of each grid hole was mapped. At each grid hole used for recording, expected depths the cortical surface, grey matter/white matter transitions, and ultimately the hippocampal region of interest were mapped prior to recording. 6. During each recording session the previously mapped values were monitored during electrode guidance towards the hippocampal region of interest. 7. In monkey R, electrode tracts were visible in a post-experimental 7T MRI acquisition. This procedure was not possible for monkey W.
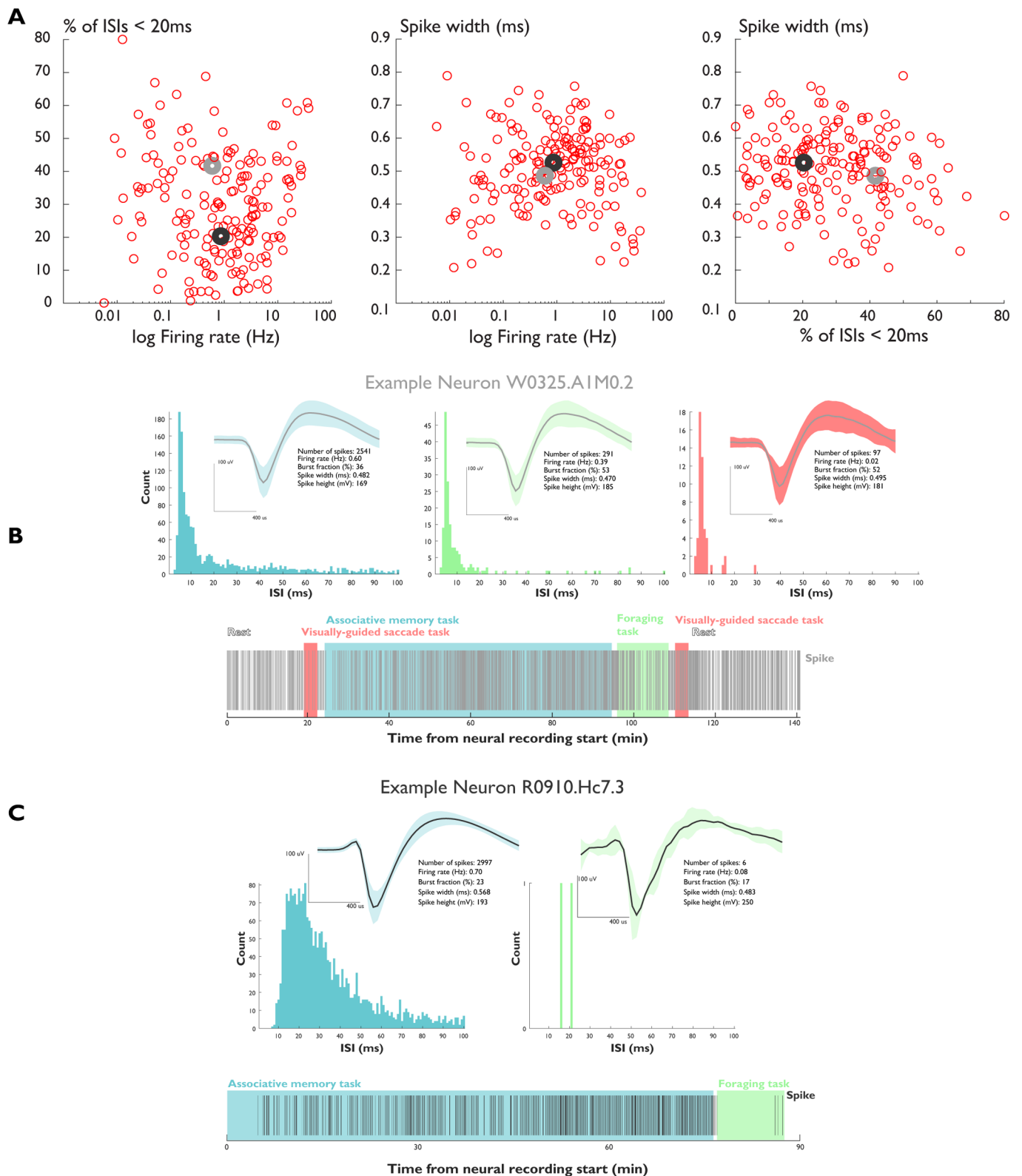
Extended Data Fig. 2 | Individual neuron characteristics and example neurons. A) Burst fraction, spike width, and firing rate of all recorded neurons ($n = 183$). Light grey circle; example neuron W0325.A1M0.2 Dark grey circle; example neuron R0910.Hc7.3. B) Example neuron W0325.A1M0.2 inter-spike-interval distribution and average waveform. Shaded area, SEM. Below, spike raster as a function of time in the experimental recording session. C) Example neuron R0910.Hc7.3 inter-spike-interval distribution and average waveform. Shaded area, SEM. Below, spike raster as a function of time in the experimental recording session.
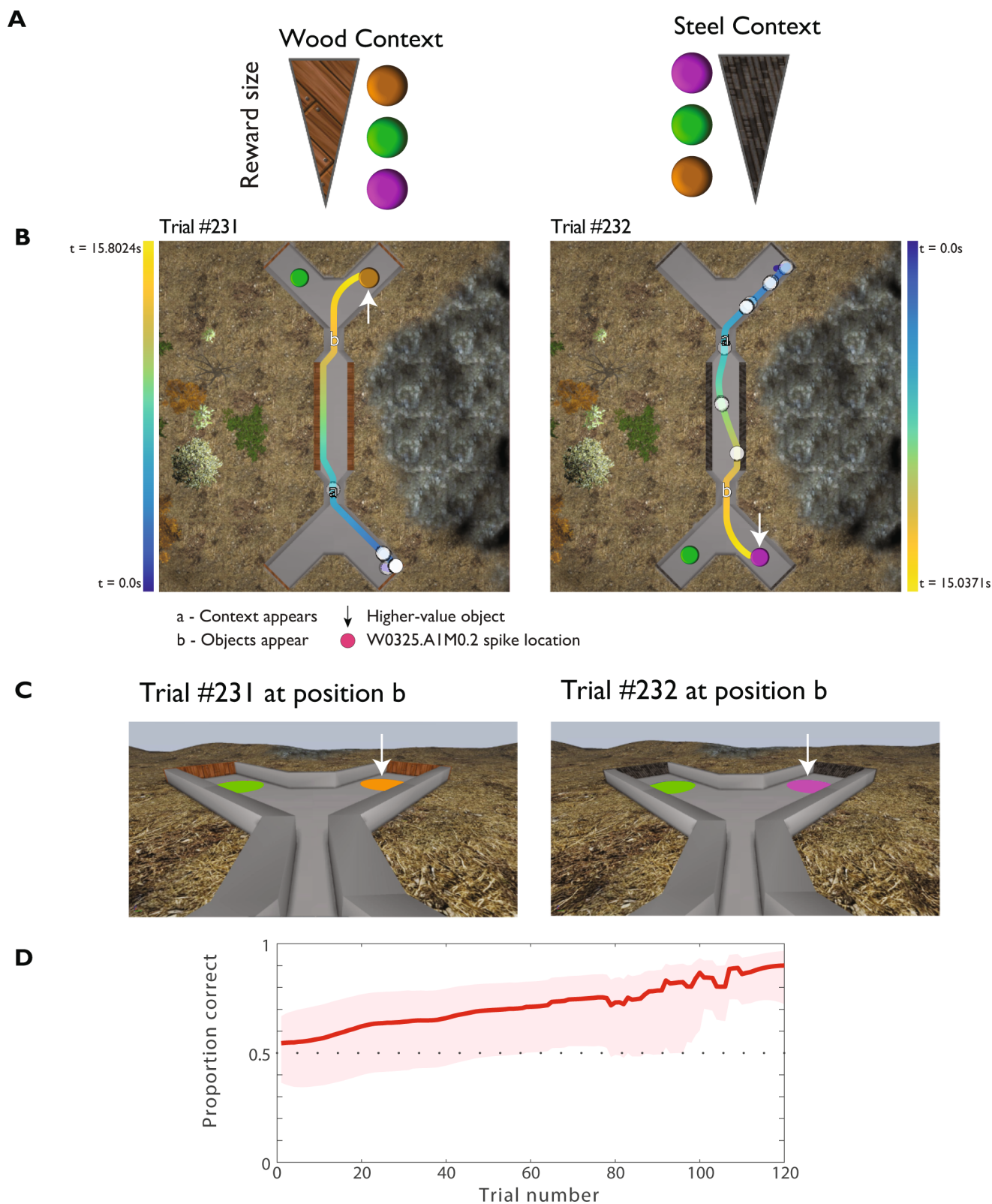
Extended Data Fig. 3 | Example associative memory task reward hierarchy. A) Example of the reversed two-context, three-object reward value hierarchy for recording session W0325. **B)** Two example trials of the associative memory task from the recording session. Subject trajectories through the maze are colored according to the time from trial start (color bar). White arrow indicates the object of higher reward value. **C)** Representative first-person-view of the monkeys during each trial at position b. White arrow indicates the object of higher reward value. **D)** Estimated learning state averaged for the high-low value context-dependent association across all sessions, and 95% confidence interval of this estimate (n=37 sessions).
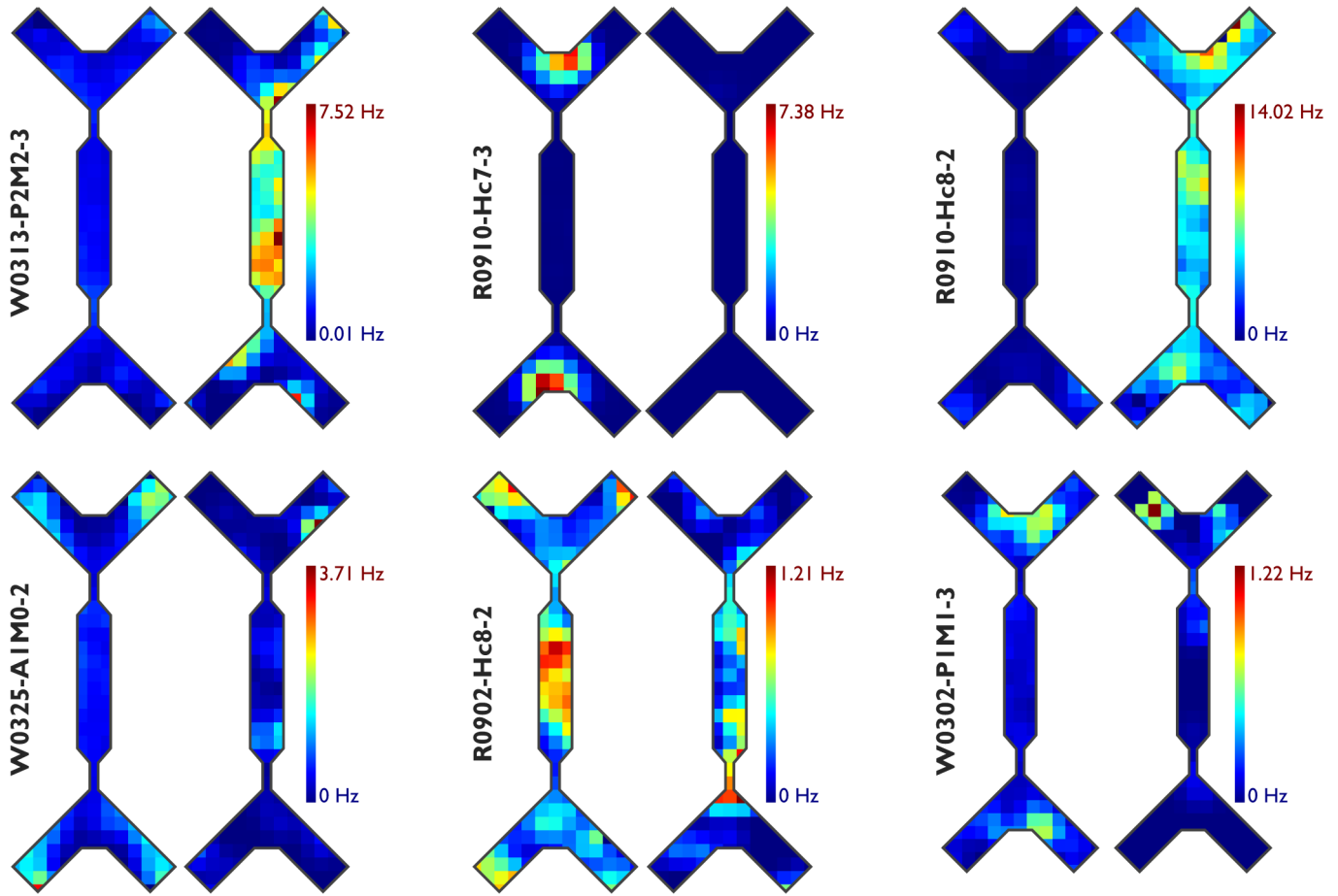
Extended Data Fig. 4 | Example neurons, smoothed firing rate maps. Smoothed firing rate maps of the six example neurons seen in Fig. 1d. Pixel-wise firing rates were smoothed with a 3-bin Gaussian kernel. Color maps are consistent within neuron and across tasks, with the maximum and minimum firing rates denoted separately for each neuron.
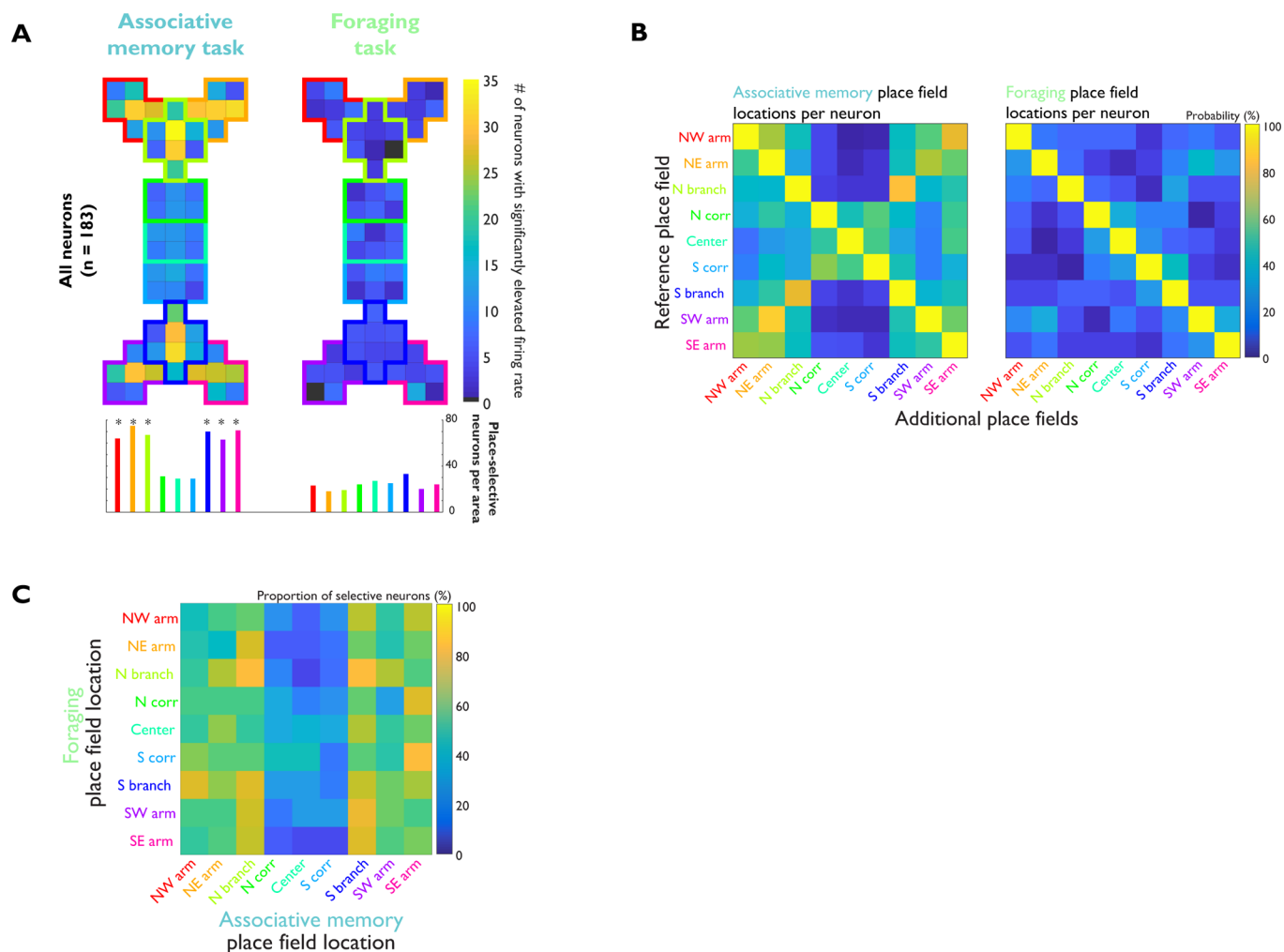
Extended Data Fig. 5 | Spatial response fields when computed with larger pixel sizes. Conventions are the same as in Fig. 2. However, all visualizations and statistics have been done with pixels that are 4 times larger. **(A)** Spatial histogram showing the number of neurons with statistically elevated firing rate in each pixel in both tasks (top). The summarized histogram (bottom) shows the number of neurons with at least one significant pixel in each maze area. *significantly different proportion across tasks; McNemar's test of equal proportions, p<0.05, Bonferroni-corrected. **(B)** Locations of coincident place fields for all neurons with more than one place field in each task. **(C)** Location of coincident place fields for all neurons with at least one place field in each task.
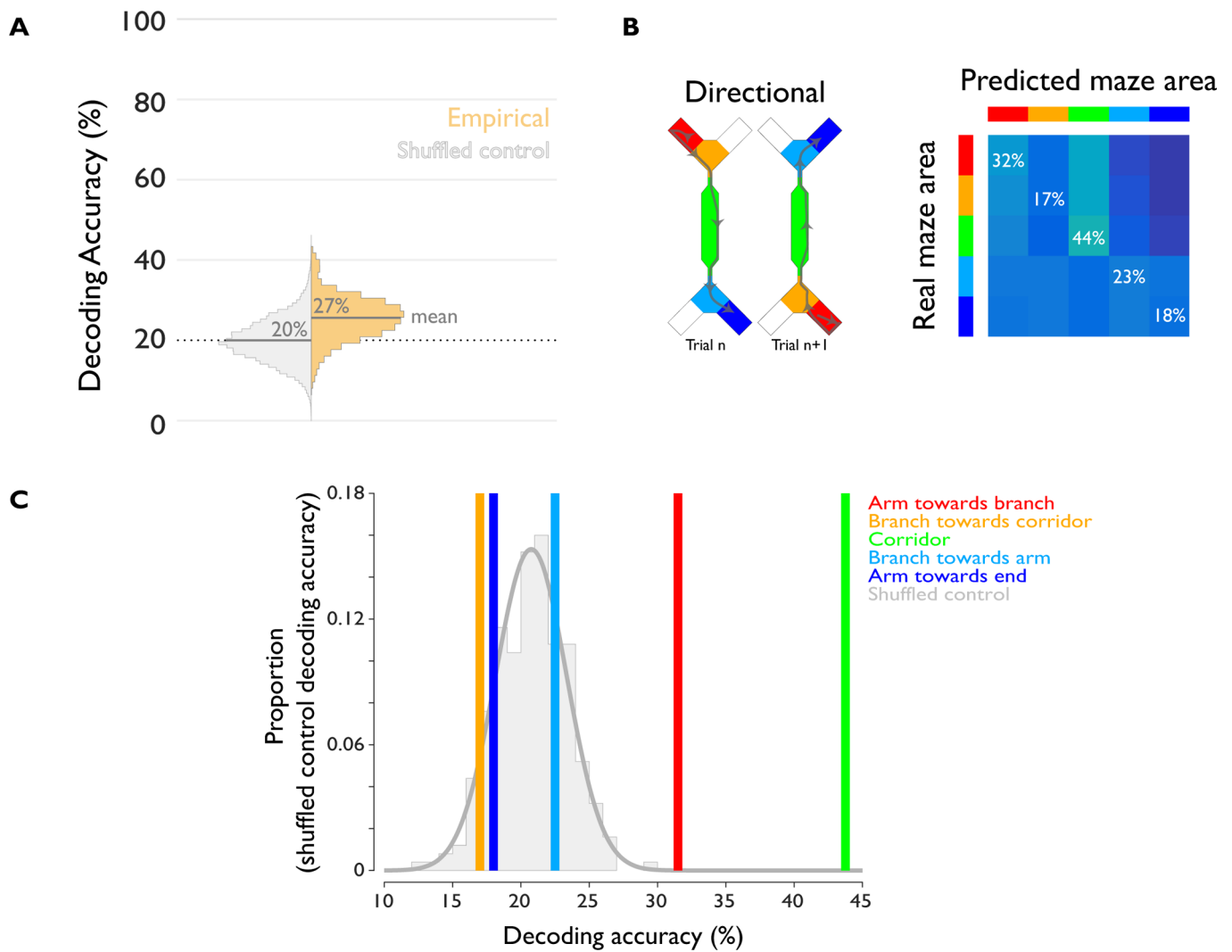
Extended Data Fig. 6 | Cross-task decoding accuracy in each area of the X-Maze. A) Cross-task decoding accuracy (orange) and decoding accuracy when the maze area labels were shuffled (also seen in Fig. 2b). Grey bars, mean. B) Confusion matrix derived from the cross-task decoding analysis (also seen in Fig. 2c). White numbers indicate the mean decoding accuracy within each maze area. C) Cross-task decoding accuracy in each maze area (colored lines) alongside the chance decoding accuracy distribution (shuffled control, grey).
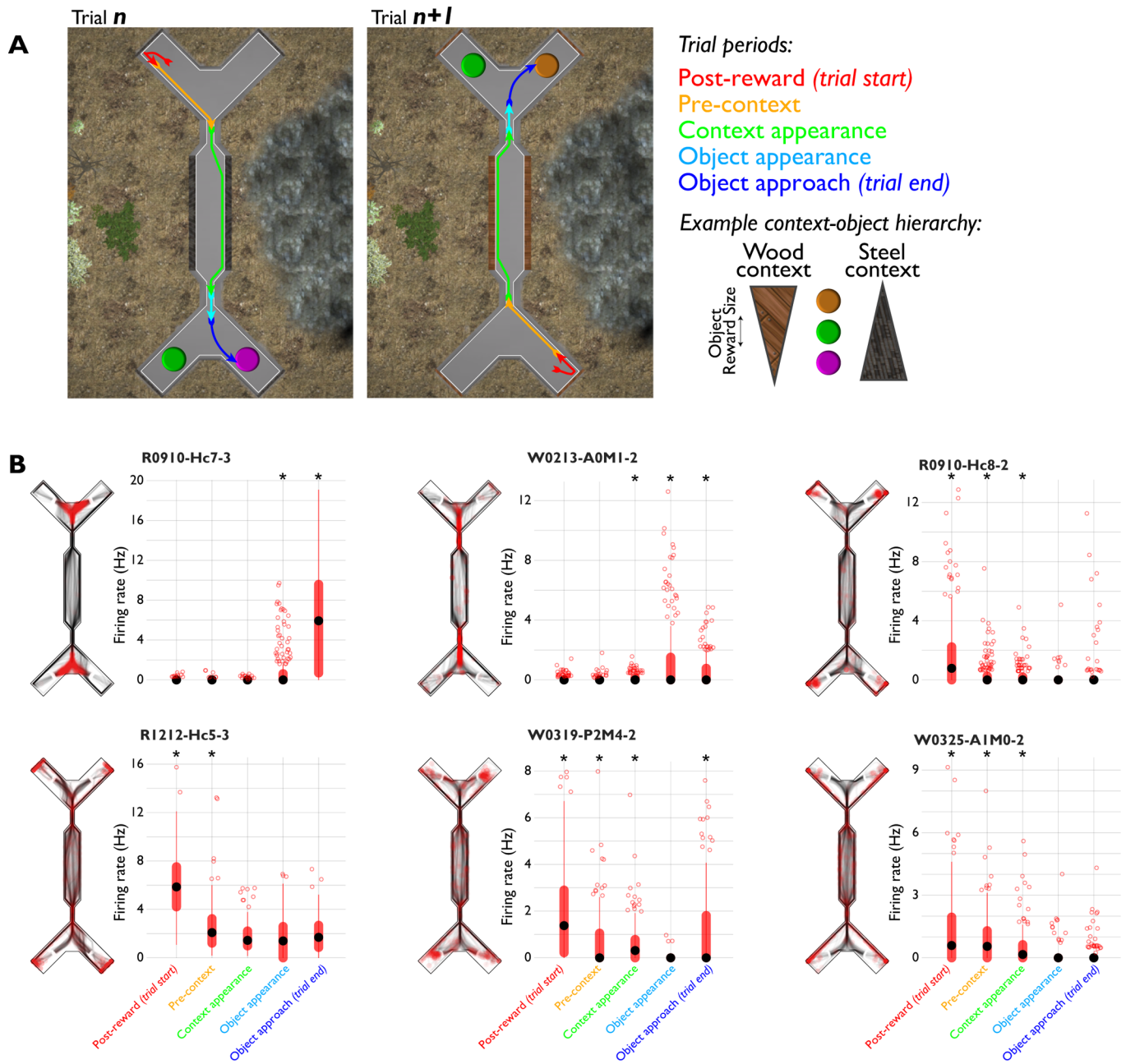
Extended Data Fig. 7 | Neuronal activity across trial epochs of the associative memory task. A) Overhead view of the X-Maze and the subject's trajectory through the maze on two consecutive trials. Each trial contains five distinct trial epochs. During the Post-reward and Pre-context epochs, all maze walls are grey and no rewarded objects are visible. Once the subject enters the central corridor, the context is cued using a wood or steel material applied to some of the maze walls. Once the subject leaves the corridor for the branched area of the maze, an object is made visible simultaneously in each arm of the maze. Subjects learn a reversed context-object reward value hierarchy by trial and error. B) Spike locations and firing rate by trial epoch for six example neurons during the associative memory task. Left: trajectories through the X-Maze (translucent grey) and spike locations (translucent red). Right: Box plot showing firing rate by trial epoch in the associative memory task. Dots indicate median value; lines indicate the 25th to 75th percentile; outliers are plotted individually. *, $p<0.05$ compared to the trial epoch with the lowest firing rate; Kruskal-Wallis, Bonferroni-corrected.
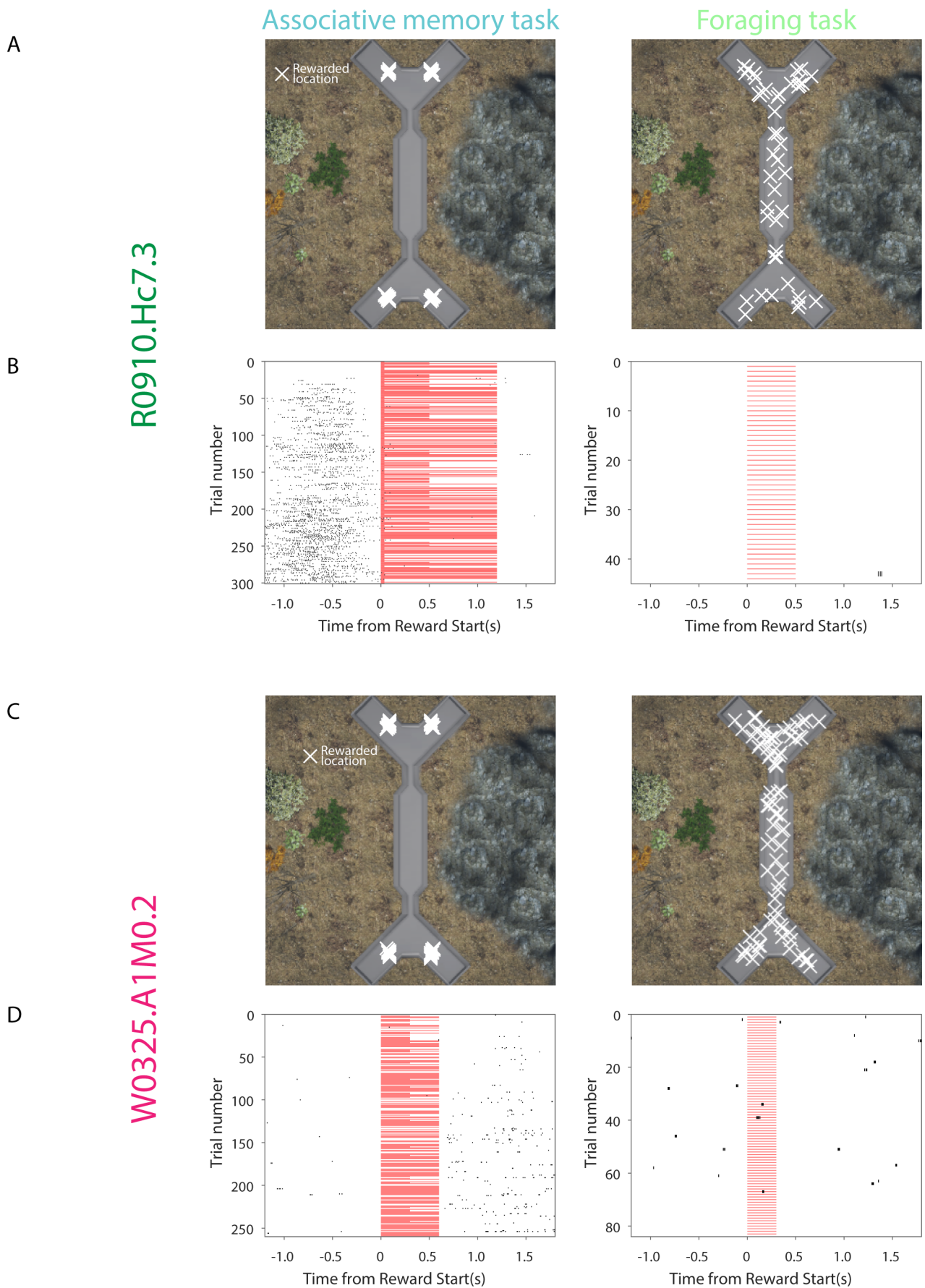
Extended Data Fig. 8 | See next page for caption.

Extended Data Fig. 8 | Rewarded-aligned spike rasters. A) Rewarded locations in session R0910 during the Associative memory task (left) and Foraging task (right). B) Reward-aligned rasters for example neuron R0910.Hc7.3 in each task. Black ticks mark the times of action potentials on each trial. The red lines mark the reward delivery for each trial. C) Rewarded locations in session W0325 during the Associative memory task (left) and Foraging task (left). D) Reward-aligned rasters for example neuron W0325.A1M0.2 in each task.
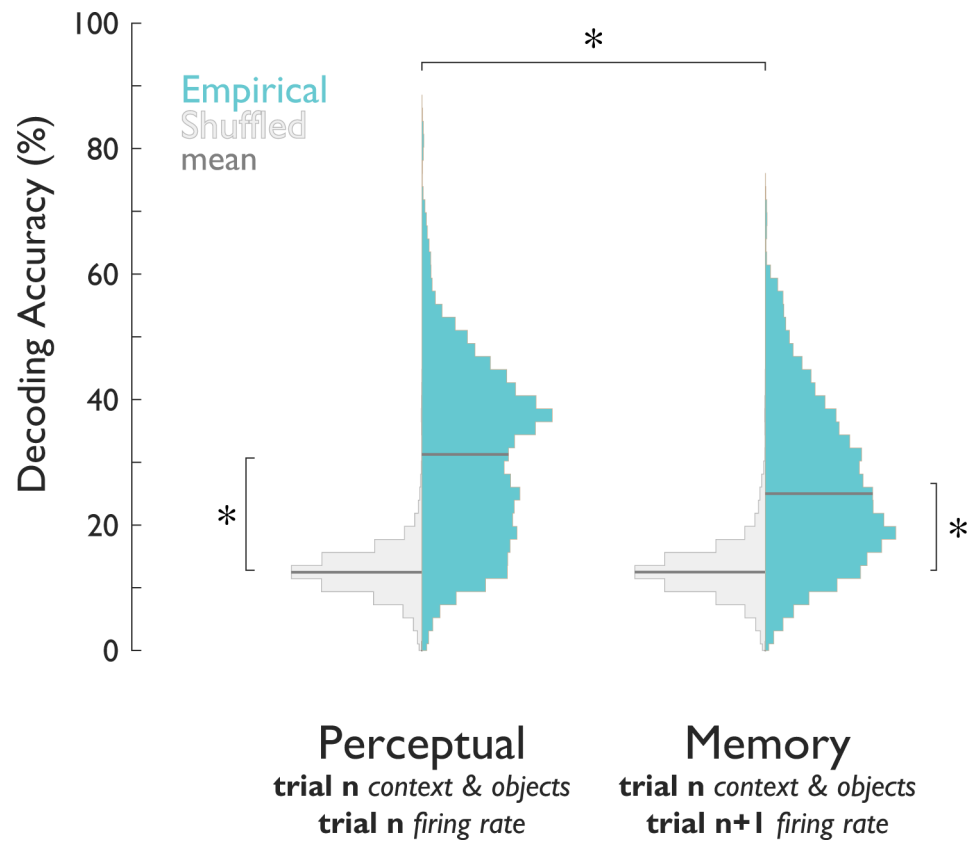
Extended Data Fig. 9 | Decoding trial type from an equal number of perceptual and mnemonic trial epochs. Distribution of classification accuracies from decoding analysis of trial type (trial context and object pair) from perceptual (object appearance, object approach) or memory (post-reward, pre-context) trial epochs in the associative memory task. *p<0.05, two-sided Wilcoxon rank-sum, n=50 per distribution. Grey bars, mean.

nature research

Corresponding author(s):   Dr. Roberto A. Gulli

Last updated by author(s): Oct 10, 2019

Reporting Summary

Nature Research wishes to improve the reproducibility of the work that we publish. This form provides structure for consistency and transparency in reporting. For further information on Nature Research policies, see Authors & Referees and the Editorial Policy Checklist.

Statistics

For all statistical analyses, confirm that the following items are present in the figure legend, table legend, main text, or Methods section.

n/a	Confirmed	
☐	☒	The exact sample size (*n*) for each experimental group/condition, given as a discrete number and unit of measurement
☐	☒	A statement on whether measurements were taken from distinct samples or whether the same sample was measured repeatedly
☐	☒	The statistical test(s) used AND whether they are one- or two-sided *Only common tests should be described solely by name; describe more complex techniques in the Methods section.*
☐	☒	A description of all covariates tested
☐	☒	A description of any assumptions or corrections, such as tests of normality and adjustment for multiple comparisons
☐	☒	A full description of the statistical parameters including central tendency (e.g. means) or other basic estimates (e.g. regression coefficient) AND variation (e.g. standard deviation) or associated estimates of uncertainty (e.g. confidence intervals)
☐	☒	For null hypothesis testing, the test statistic (e.g. *F*, *t*, *r*) with confidence intervals, effect sizes, degrees of freedom and *P* value noted *Give P values as exact values whenever suitable.*
☒	☐	For Bayesian analysis, information on the choice of priors and Markov chain Monte Carlo settings
☒	☐	For hierarchical and complex designs, identification of the appropriate level for tests and full reporting of outcomes
☐	☒	Estimates of effect sizes (e.g. Cohen's *d*, Pearson's *r*), indicating how they were calculated

Our web collection on statistics for biologists contains articles on many of the points above.

Software and code

Policy information about availability of computer code

Data collection	Data were recorded using software from Blackrock Microsystems (Cerebus Software Suite, version XX). Neuronal data were sorted using Offline Sorter v2, from Plexon. Virtual enivironments were built using Unreal Engine (May 2012 release), and Matlab (2013b), as described in Doucet, Gulli & Martinez-Trujillo (J Neurosci Methods, 2016).
Data analysis	All data were analyed uzing custom code written in Matlab (2018a). All code is available upon request.

For manuscripts utilizing custom algorithms or software that are central to the research but not yet described in published literature, software must be made available to editors/reviewers. We strongly encourage code deposition in a community repository (e.g. GitHub). See the Nature Research guidelines for submitting code & software for further information.

Data

Policy information about availability of data

All manuscripts must include a data availability statement. This statement should provide the following information, where applicable:
- Accession codes, unique identifiers, or web links for publicly available datasets
- A list of figures that have associated raw data
- A description of any restrictions on data availability

Data accession codes will be provided at the proof stage (per conversation with Dr. Dhruv)

Field-specific reporting

Please select the one below that is the best fit for your research. If you are not sure, read the appropriate sections before making your selection.

☒ Life sciences   ☐ Behavioural & social sciences   ☐ Ecological, evolutionary & environmental sciences

For a reference copy of the document with all sections, see nature.com/documents/nr-reporting-summary-flat.pdf

Life sciences study design

All studies must disclose on these points even when the disclosure is negative.

Sample size	Analyses of single neurons were carried out on a population of 183 neurons, consistent with the sample size of previously published work (Wirth et al. 2003, Science). Population decoding analyses were carried out using a sample of 152 neurons.
Data exclusions	Neurons were excluded from the larger population with fewer than 10 traversals of each maze area in either task to allow for splitting the data into adequately sized training and test sets for classification analyses.
Replication	All analyses were conducted independently in both monkeys; qualitative differences between monkeys were not observed.
Randomization	In this study design, randomization of conditions was not applicable; all subjects participated in all conditions (i.e. tasks).
Blinding	Experiments could not be conducted in a blinded manner, since experimenters needed to actively monitor behaviour of the subjects. Analyses were conducted in a manner that was agnostic to condition; the same code was used to run analyses of data generated in both tasks.

Reporting for specific materials, systems and methods

We require information from authors about some types of materials, experimental systems and methods used in many studies. Here, indicate whether each material, system or method listed is relevant to your study. If you are not sure if a list item applies to your research, read the appropriate section before selecting a response.

Materials & experimental systems

n/a	Involved in the study
☒	☐ Antibodies
☒	☐ Eukaryotic cell lines
☒	☐ Palaeontology
☐	☒ Animals and other organisms
☒	☐ Human research participants
☒	☐ Clinical data

Methods

n/a	Involved in the study
☒	☐ ChIP-seq
☒	☐ Flow cytometry
☒	☐ MRI-based neuroimaging

Animals and other organisms

Policy information about studies involving animals; ARRIVE guidelines recommended for reporting animal research

Laboratory animals	2 male Macaca mulatta (7 years old, 7 kg; 14 years old, 12 kg)
Wild animals	None
Field-collected samples	None
Ethics oversight	McGill University Animal Care Committee, Canadian Committee for Animal Care

Note that full information on the approval of the study protocol must also be provided in the manuscript.